

OPERATING CHARACTERISTICS OF A
URANIUM GRAPHITE SUBCRITICAL
ASSEMBLY WITH COOLANT SIMULATION

John Henry Hoganson

500-

er for ol

OPERATING CHARACTERISTICS OF A
URANIUM GRAPHITE SUBCRITICAL ASSEMBLY
WITH COOLANT SIMULATION

by

John Henry Hoganson

A Thesis Submitted to the
Graduate Faculty in Partial Fulfillment of
The Requirements for the Degree of
MASTER OF SCIENCE

Major Subject: Engineering

TABLE OF CONTENTS

	Page
I. INTRODUCTION	1
II. REVIEW OF LITERATURE	4
III. THEORETICAL ANALYSIS	7
A. General Procedure	7
B. Fast Fission Factor	8
C. Primary Fission Neutrons	10
D. Thermal Utilization	12
1. Method A	12
2. Method B	20
E. Resonance Escape Probability	25
1. Method A	25
2. Method B	29
F. Buckling	31
IV. EXPERIMENTAL INVESTIGATION	33
A. Description of Equipment	33
B. Procedure	36
V. RESULTS	41
VI. DISCUSSION OF RESULTS	49
VII. CONCLUSIONS	52
VIII. LITERATURE CITED	77
IX. ACKNOWLEDGEMENTS	79
X. APPENDIX	80

CONTENTS

1	INTRODUCTION	1
2	THEORY OF THE SUBJECT	2
3	THEORY OF THE SUBJECT	3
4	THEORY OF THE SUBJECT	4
5	THEORY OF THE SUBJECT	5
6	THEORY OF THE SUBJECT	6
7	THEORY OF THE SUBJECT	7
8	THEORY OF THE SUBJECT	8
9	THEORY OF THE SUBJECT	9
10	THEORY OF THE SUBJECT	10
11	THEORY OF THE SUBJECT	11
12	THEORY OF THE SUBJECT	12
13	THEORY OF THE SUBJECT	13
14	THEORY OF THE SUBJECT	14
15	THEORY OF THE SUBJECT	15
16	THEORY OF THE SUBJECT	16
17	THEORY OF THE SUBJECT	17
18	THEORY OF THE SUBJECT	18
19	THEORY OF THE SUBJECT	19
20	THEORY OF THE SUBJECT	20
21	THEORY OF THE SUBJECT	21
22	THEORY OF THE SUBJECT	22
23	THEORY OF THE SUBJECT	23
24	THEORY OF THE SUBJECT	24
25	THEORY OF THE SUBJECT	25
26	THEORY OF THE SUBJECT	26
27	THEORY OF THE SUBJECT	27
28	THEORY OF THE SUBJECT	28
29	THEORY OF THE SUBJECT	29
30	THEORY OF THE SUBJECT	30
31	THEORY OF THE SUBJECT	31
32	THEORY OF THE SUBJECT	32
33	THEORY OF THE SUBJECT	33
34	THEORY OF THE SUBJECT	34
35	THEORY OF THE SUBJECT	35
36	THEORY OF THE SUBJECT	36
37	THEORY OF THE SUBJECT	37
38	THEORY OF THE SUBJECT	38
39	THEORY OF THE SUBJECT	39
40	THEORY OF THE SUBJECT	40
41	THEORY OF THE SUBJECT	41
42	THEORY OF THE SUBJECT	42
43	THEORY OF THE SUBJECT	43
44	THEORY OF THE SUBJECT	44
45	THEORY OF THE SUBJECT	45
46	THEORY OF THE SUBJECT	46
47	THEORY OF THE SUBJECT	47
48	THEORY OF THE SUBJECT	48
49	THEORY OF THE SUBJECT	49
50	THEORY OF THE SUBJECT	50
51	THEORY OF THE SUBJECT	51
52	THEORY OF THE SUBJECT	52
53	THEORY OF THE SUBJECT	53
54	THEORY OF THE SUBJECT	54
55	THEORY OF THE SUBJECT	55
56	THEORY OF THE SUBJECT	56
57	THEORY OF THE SUBJECT	57
58	THEORY OF THE SUBJECT	58
59	THEORY OF THE SUBJECT	59
60	THEORY OF THE SUBJECT	60
61	THEORY OF THE SUBJECT	61
62	THEORY OF THE SUBJECT	62
63	THEORY OF THE SUBJECT	63
64	THEORY OF THE SUBJECT	64
65	THEORY OF THE SUBJECT	65
66	THEORY OF THE SUBJECT	66
67	THEORY OF THE SUBJECT	67
68	THEORY OF THE SUBJECT	68
69	THEORY OF THE SUBJECT	69
70	THEORY OF THE SUBJECT	70
71	THEORY OF THE SUBJECT	71
72	THEORY OF THE SUBJECT	72
73	THEORY OF THE SUBJECT	73
74	THEORY OF THE SUBJECT	74
75	THEORY OF THE SUBJECT	75
76	THEORY OF THE SUBJECT	76
77	THEORY OF THE SUBJECT	77
78	THEORY OF THE SUBJECT	78
79	THEORY OF THE SUBJECT	79
80	THEORY OF THE SUBJECT	80
81	THEORY OF THE SUBJECT	81
82	THEORY OF THE SUBJECT	82
83	THEORY OF THE SUBJECT	83
84	THEORY OF THE SUBJECT	84
85	THEORY OF THE SUBJECT	85
86	THEORY OF THE SUBJECT	86
87	THEORY OF THE SUBJECT	87
88	THEORY OF THE SUBJECT	88
89	THEORY OF THE SUBJECT	89
90	THEORY OF THE SUBJECT	90
91	THEORY OF THE SUBJECT	91
92	THEORY OF THE SUBJECT	92
93	THEORY OF THE SUBJECT	93
94	THEORY OF THE SUBJECT	94
95	THEORY OF THE SUBJECT	95
96	THEORY OF THE SUBJECT	96
97	THEORY OF THE SUBJECT	97
98	THEORY OF THE SUBJECT	98
99	THEORY OF THE SUBJECT	99
100	THEORY OF THE SUBJECT	100

I. INTRODUCTION

The maximum power level of a nuclear reactor is frequently limited by the rate of heat removal. The actual design of a power reactor represents a compromise between the requirements of heat transfer and those of nuclear physics. Nuclear reactor theory is not sufficiently accurate to guarantee that a particular reactor (especially one of a new design) will go critical. Therefore, the nuclear characteristics of a reactor design must be obtained before construction of the full scale reactor. Some of this information can be obtained from the use of a subcritical assembly.

Experiments with uranium graphite subcritical assemblies can be carried out to determine the various nuclear constants of a proposed reactor lattice. These lattice constants are the material buckling, multiplication constant, lattice diffusion length, and thermal utilization of the unit cell including the process tube assembly.

In this investigation six lattice configurations were considered, and the buckling of each was determined experimentally. Lattice cells of 6 in., 8.5 in., and 12 in., denoted I, II, and III respectively, constituted the three geometric lattice arrangements. For each of these, both the "wet" and "dry" cases were considered. The measurements and calculations with water present in the cooling annulus were

designated as "wet", and those with the process tube, but without water, as "dry".

These six lattice configurations were also considered in the theoretical analysis. The buckling of each of the six lattice configurations was determined theoretically by two methods. Only one size fuel element and one size process tubing was used in the experimental and theoretical analyses of this investigation.

The methods of Murray (1) and of Rumsey and Volkoff (2), (3) were used to determine theoretically the thermal utilization and the resonance escape probability. Murray's method was shown to give less conservative results than the method of Rumsey and Volkoff. The theoretical multiplication constant derived for each configuration considered was based on literature and calculated values of the various diffusion lengths, the Fermi age, and the various macroscopic cross sections. The product of η and ϵ was assumed to be essentially constant for the various configurations investigated.

Analyses of the data for the given configurations were carried out by use of the classical formula for the buckling

$$B^2 = \frac{\eta \epsilon p f - 1}{L^2 + \eta \epsilon p f \tau} \quad (1)$$

A comparison between the "wet" and "dry" cases of the three lattice cells considered was presented using the experimental and theoretical values of the buckling. By an analysis of the results obtained in this investigation, the effect of the water coolant on the nuclear properties of the various lattice configurations was determined.

II. REVIEW OF LITERATURE

The theoretical calculation of the multiplication factor for a heterogeneous reactor with coolant is an extension to the method of calculating the thermal utilization and resonance escape probability factors for an infinite heterogeneous uranium-graphite reactor presented by Weinberg (4), (5). Guggenheim and Pryce (6) extended the method to include a non-absorbing coolant and a thin sheath of absorbant aluminum around the fuel element. Houston (7) extended the method to include neutron absorption in a coolant. Houston's results are more suitable for gas or heavy liquid metal cooled reactors due to his assumptions concerning the coolant's negligible moderating properties and small volume fraction of the lattice cell. Rumsey and Volkoff (2), (3) extended the above methods further to include the moderating effect of a water annulus.

Murray (1) presented a simplified method of calculating the thermal utilization which considers all but the uranium and the graphite in the lattice cell as poisons which reduce the basic uranium graphite thermal utilization. Murray's method for the calculation of the resonance escape probability does not consider the so called poisons. The Rumsey and Volkoff method appears to be at the present time the most comprehensive theoretical analysis of a water cooled uranium-graphite lattice cell.

The experiments with subcritical assemblies of the Hanford Atomic Products Operation included an effort to determine the effect of a water annulus around the fuel element on the buckling. The effect of aluminum, air, and other impurities in the lattice upon the buckling was also investigated (8). A few measurements were taken using internally cooled cylindrical fuel rods, but the majority of the coolant simulation experiments were with solid cylindrical fuel rods of natural uranium surrounded by an annulus of water. The objectives of the subcritical assembly experiments at Hanford (3) were to determine experimentally the various lattice constants. The existing lattice theory was supplemented and improved where possible. Lattice measurements were taken with three different fuel rod diameters: 0.925 in., 1.175 in., and 1.36 in. The lattice spacing and the water-aluminum-uranium ratios were varied for each slug size.

The results of the series of tests using both "wet" and "dry" lattices were compiled by Clayton (9). A comparison of theory and experimental results for one fuel element diameter, six lattice spacings, and the "wet" and "dry" configurations for the Hanford Atomic Products Operation was done by Gast and others (2). Gast used the method of Rumsey and Volkoff to calculate the theoretical values of the thermal utilization and the resonance escape probability.

Related conclusions (8) from the Hanford work with water cooled uranium graphite lattices were:

- (a) For a given natural uranium fuel assembly, there is a maximum in the buckling vs. C/U atom ratio curve. The slug diameter and the water annulus thickness are inversely proportional to the value of C/U at which the maximum occurs. This maximum occurs between C/U values of 50 and 100.
- (b) The buckling "dry" is greater than the buckling "wet" for larger lattice spacings (C/U atom ratio). As the lattice spacing is decreased, the buckling curves cross and the "wet" buckling becomes greater than the "dry" buckling. For this lower C/U atom ratio region, externally cooled slugs exhibit a "fail-safe" behavior on the loss of water.

The following conclusions were a result of the Hanford experiments(2). The state of the heterogeneous graphite uranium lattice theory at present is not completely satisfactory. More experimental measurements of individual parameters such as f and p are necessary in order to establish the basis for an improved theoretical analysis. Corrections for variations in reactor material densities and purities, and allowances for holes, such as for control rods, need further investigation (2). Finally, the treatment of the energy spectrum of neutrons, fast to thermal, requires more accurate development of neutron resonance and capture reactions.

III. THEORETICAL ANALYSIS

A. General Procedure

The product of the fast fission factor, ϵ , the primary fission neutron factor, η , the thermal utilization factor, f , and the resonance escape factor, p , is the infinite multiplication constant, k_{∞} .

$$\epsilon \eta f p = k_{\infty} \quad (2)$$

A theoretical analysis of each of the factors would have been extremely complicated without certain simplifying assumptions. These assumptions are stated where applicable in the following theory. Each of the factors was considered separately. The product $\epsilon \eta$ was determined and assumed constant for all the lattice configurations considered. Expressions for f and p were determined using the methods of Murray, denoted Method A, and the methods of Rumsey and Volkoff, denoted Method B, for the "wet" and "dry" cases of Lattices I, II and III.

Using values from the literature for the lattice diffusion length and the Fermi age with the theoretically determined infinite multiplication constant, the buckling was determined from Equation 1. The theoretical buckling was determined

THE UNIVERSITY OF CHICAGO

1. General Remarks

The present work is a study of the history of the University of Chicago from its founding in 1837 to the present. It is a history of the University as an institution, and not a history of the University as a collection of individuals. The history of the University is a history of the University as an institution, and not a history of the University as a collection of individuals.

(2) ∞ π ∞

1. General Remarks. The history of the University of Chicago is a history of the University as an institution, and not a history of the University as a collection of individuals. The history of the University is a history of the University as an institution, and not a history of the University as a collection of individuals. The history of the University is a history of the University as an institution, and not a history of the University as a collection of individuals.

2. General Remarks. The history of the University of Chicago is a history of the University as an institution, and not a history of the University as a collection of individuals. The history of the University is a history of the University as an institution, and not a history of the University as a collection of individuals. The history of the University is a history of the University as an institution, and not a history of the University as a collection of individuals.

for Lattices I, II, and III for both the "wet" and "dry" cases using both Methods A and B.

The effect of the air annulus and air holes on the neutron density in all lattice geometries was neglected due to the magnitude of the effect in comparison with other material effects in the lattice.

Subscripts used in this analysis were defined as follows:

u	natural uranium
al	slug can, 2S aluminum
w	water
g	graphite
m	moderator
p	process tube, 61S aluminum
a	absorption
s	scattering
re	resonance
sa	scattering "absorption"
f	slow neutron fission
t	transport theory

Any deviation of notation from the above list was individually defined.

B. Fast Fission Factor

The fast fission factor, ϵ , is the ratio of the total number of neutrons produced by fission to the number of neutrons

for 'edition 1' (1971) and 'edition 2' (1972)

later using both editions 1 and 2

The effect of the two editions on the data is shown

from density to all classes (percentage of total area)

the results of the two editions are compared with the results

of the two editions

The results of the two editions are compared with the results

of the two editions

of the two editions

of the two editions

of the two editions

of the two editions

of the two editions

of the two editions

of the two editions

of the two editions

of the two editions

of the two editions

of the two editions

of the two editions

of the two editions

of the two editions

of the two editions

of the two editions

of the two editions

produced by fission by thermal neutrons. Assuming that the primary neutron source is distributed approximately uniformly over the fuel, a simplified version of the equation given by Glasstone and Edlund (5, p. 278) for the fast fission factor is

$$\epsilon - 1 = \frac{\left[(\nu - 1) - \frac{\sigma_e}{\sigma_f} \right] \frac{\sigma_f}{\sigma_t} P}{1 - P \left(\frac{\nu \sigma_f + \sigma_e}{\sigma_t} \right)} = \frac{(\eta - 1) \frac{\sigma_a}{\sigma_t} P}{1 - \frac{P}{\sigma_t} (\eta \sigma_a + \sigma_e)} \quad (3)$$

where P is the probability that a fission neutron born in a rod will make a collision inside the rod in which it was created;

σ_a is the absorption cross section for fast neutrons, that is, the sum of the fission and the capture cross sections;

σ_e is the elastic cross section for fast neutrons;

σ_i is the inelastic cross section for fast neutrons;

and σ_t is the total cross section for fast neutrons.

$$\sigma_t = \sigma_a + \sigma_e + \sigma_i.$$

Using fast neutron cross section values as given by Guggenheim and Pryce (6, p. 51), Equation 3 reduces to

$$\epsilon - 1 = \frac{0.0948 P}{1 - 0.521 P} \quad (4)$$

These numerical coefficients are such that when the fuel element radius is less than 1.7 cm the calculated value of ϵ agrees reasonably well with experimental results obtained by Argonne National Laboratory (6, p.51). For natural uranium of density 19 g/cm^3 and a rod radius of 0.5 in., the value of $N\sigma_t r_u$ is 0.262, where N is the number of uranium atoms per unit volume, and r_u is the radius of the fuel rod. The quantity P is a function of $N\sigma_t r_u$. From a relationship of P and $N\sigma_t r_u$ shown by Guggenheim and Pryce (6, p. 51) and the above computed value of $N\sigma_t r_u$, the value of P determined was 0.25.

Solving Equation 4 for ϵ gave a value of 1.027. This value for the fast fission factor was assumed constant for all configurations investigated.

C. Primary Fission Neutrons

The number of fission neutrons released per thermal neutron captured in the fuel is the factor, η . Glasstone and Edlund define η (5, p. 83) as

$$\eta = \frac{\nu \sum_f^u}{\sum_a^u} \quad (5)$$

where ν is the average number of neutrons produced per thermal neutron fission;

and Σ_a is the total cross section for absorption of thermal neutrons.

The microscopic thermal fission cross section for natural uranium is 4.18 barns. Applying the maxwellian distribution correction of 1.128 and the "not - $1/v$ " factor of 0.981 for U^{235} to this value gives an effective fission cross section of 3.635 barns for natural uranium. The microscopic thermal absorption cross section for natural uranium is 7.68 barns. Applying the maxwellian distribution correction and a "not - $1/v$ " factor of 0.990 for natural uranium to this value determines an effective absorption cross section of 6.74 barns for natural uranium (1, p. 32).

Murray (1, p. 98) gives a value of 2.46 for ν . Substituting the above quantities in Equation 5, the calculated value of η was 1.327.

It is normal practice in working with subcritical assemblies to experimentally determine k_{∞} and then divide k_{∞} by the product ϵpf to arrive at a value of η . The value of η found by subcritical assembly experiments was 1.308 neutrons per thermal neutron captured (10, p. 85). This value is in reasonable agreement to the computed value of 1.327. The value of η used in the following analysis was 1.308 and was assumed constant for all configurations investigated.

THESE RESULTS ARE IN ACCORD WITH THE RESULTS OF OTHER

WORKERS IN THIS FIELD AND ARE IN GOOD AGREEMENT WITH

THE RESULTS OF OTHER WORKERS IN THIS FIELD AND ARE

IN GOOD AGREEMENT WITH THE RESULTS OF OTHER WORKERS

IN THIS FIELD AND ARE IN GOOD AGREEMENT WITH THE

RESULTS OF OTHER WORKERS IN THIS FIELD AND ARE

IN GOOD AGREEMENT WITH THE RESULTS OF OTHER WORKERS

IN THIS FIELD AND ARE IN GOOD AGREEMENT WITH THE

RESULTS OF OTHER WORKERS IN THIS FIELD AND ARE

IN GOOD AGREEMENT WITH THE RESULTS OF OTHER WORKERS

IN THIS FIELD AND ARE IN GOOD AGREEMENT WITH THE

RESULTS OF OTHER WORKERS IN THIS FIELD AND ARE

IN GOOD AGREEMENT WITH THE RESULTS OF OTHER WORKERS

IN THIS FIELD AND ARE IN GOOD AGREEMENT WITH THE

RESULTS OF OTHER WORKERS IN THIS FIELD AND ARE

IN GOOD AGREEMENT WITH THE RESULTS OF OTHER WORKERS

IN THIS FIELD AND ARE IN GOOD AGREEMENT WITH THE

RESULTS OF OTHER WORKERS IN THIS FIELD AND ARE

IN GOOD AGREEMENT WITH THE RESULTS OF OTHER WORKERS

IN THIS FIELD AND ARE IN GOOD AGREEMENT WITH THE

RESULTS OF OTHER WORKERS IN THIS FIELD AND ARE

IN GOOD AGREEMENT WITH THE RESULTS OF OTHER WORKERS

D. Thermal Utilization

In heterogeneous lattice theory the finite lattice reactor is assumed to be an infinite lattice array. The problem of calculating k and ρ is simplified by replacing the square cells by equivalent cylindrical unit cells. Table 1 gives the equivalent cell dimensions for Lattices I, II, and III. Assuming that little change in the overall neutron flux is experienced in traversing one cell, an individual cell may be representative of the total.

The methods of Murray (1) and of Rumsey and Volkoff (2), (3) were used to determine theoretically the thermal utilization. These methods were considered separately and were denoted Methods A and B respectively.

1. Method A

The depression of the thermal neutron flux in the fuel and adjacent moderator complicates the calculation of the thermal utilization. Average flux and volume weighting factors must both be included in the fractional absorption of the fuel. From the spatial variation of the flux in a cell, the average values of the flux can be determined.

The thermal neutron diffusion equations for the uranium and the moderator from diffusion theory are

$$D_u \nabla^2 \phi_u - \phi_u \Sigma_u + S_u = 0 \quad (6)$$

and

$$D_m \nabla^2 \phi_m - \phi_m \sum_m + S_m = 0 \quad (7)$$

Equations 6 and 7 can be simplified with the following assumptions:

- (a) The variation of neutron flux at a given cell radius will be the same everywhere.
- (b) There are no thermal neutrons produced in the uranium. S_u is zero.
- (c) The production rate of thermal neutrons in the moderator is independent of position. S_m is constant.
- (d) The flux is assumed not to vary along the fuel cell axis.

Using the above assumptions and cylindrical coordinates, Equation 6 for the fuel becomes

$$\frac{d^2 \phi_u}{dx^2} + \frac{1}{x} \left(\frac{d\phi_u}{dx} \right) - \phi_u = 0 \quad (8)$$

where $x = H_u r$ and H_u is the inverse diffusion length of uranium, and Equation 7 for the moderator becomes

$$\frac{d^2 \phi_m}{dr^2} + \frac{1}{r} \left(\frac{d\phi_m}{dr} \right) - H_m^2 \phi_m = - \frac{S_m}{D_m} \quad (9)$$

(1)

$$x = \sum_{i=1}^n x_i \quad \text{and} \quad y = \sum_{i=1}^n y_i$$

Let x and y be two vectors in \mathbb{R}^n . Then x and y are orthogonal if and only if $x \cdot y = 0$.

(2) Let x and y be two vectors in \mathbb{R}^n . Then x and y are parallel if and only if $x = cy$ for some scalar c .

(3) Let x and y be two vectors in \mathbb{R}^n . Then x and y are linearly independent if and only if x and y are not parallel.

(4) Let x and y be two vectors in \mathbb{R}^n . Then x and y are linearly dependent if and only if x and y are parallel.

(5) Let x and y be two vectors in \mathbb{R}^n . Then x and y are orthogonal if and only if $x \cdot y = 0$.

(6) Let x and y be two vectors in \mathbb{R}^n . Then x and y are parallel if and only if $x = cy$ for some scalar c .

(7) Let x and y be two vectors in \mathbb{R}^n . Then x and y are linearly independent if and only if x and y are not parallel.

(8) Let x and y be two vectors in \mathbb{R}^n . Then x and y are linearly dependent if and only if x and y are parallel.

(9) Let x and y be two vectors in \mathbb{R}^n . Then x and y are orthogonal if and only if $x \cdot y = 0$.

(10) Let x and y be two vectors in \mathbb{R}^n . Then x and y are parallel if and only if $x = cy$ for some scalar c .

(11) Let x and y be two vectors in \mathbb{R}^n . Then x and y are linearly independent if and only if x and y are not parallel.

(12) Let x and y be two vectors in \mathbb{R}^n . Then x and y are linearly dependent if and only if x and y are parallel.

(13)

$$x = \sum_{i=1}^n x_i \quad \text{and} \quad y = \sum_{i=1}^n y_i$$

Let x and y be two vectors in \mathbb{R}^n . Then x and y are orthogonal if and only if $x \cdot y = 0$.

(14) Let x and y be two vectors in \mathbb{R}^n . Then x and y are parallel if and only if $x = cy$ for some scalar c .

(15)

$$x = \sum_{i=1}^n x_i \quad \text{and} \quad y = \sum_{i=1}^n y_i$$

where D_m is the diffusion coefficient for the moderator.

κ_m^2 is the square of the inverse diffusion length.

Equation 8 for the fuel is the modified Bessel equation of zero order. Equation 9 for the moderator is the inhomogeneous type of the modified Bessel equation of zero order. The solutions of Equations 8 and 9 are

$$\phi_u(r) = A I_0 (\kappa_u r) \quad (10)$$

$$\text{and} \quad \phi_m(r) = C K_0 (\kappa_m r) + G I_0 (\kappa_m r) + \frac{S_m}{\Sigma_m} \quad (11)$$

respectively. The boundary conditions used in the evaluation of the constants A , C , and G are neutron flux and current continuity at $r = r_u$ (uranium rod radius) and the condition that $d\phi_m/dr = 0$ at $r = r_2$ (the equivalent outer radius of the graphite cell).

Applying the condition of zero neutron current at r_2 in Equation 11

$$G = C \frac{K_1 (\kappa_m r_2)}{I_1 (\kappa_m r_2)} \quad (12)$$

thus the moderator flux, Equation 11, becomes

$$\phi_m(r) = C M_0 (\kappa_m r) + \frac{S_m}{\Sigma_m} \quad (13)$$

where

$$M_0(\phi_m r) = K_0(\phi_m r) + \frac{K_1(\phi_m r_2)}{I_1(\phi_m r_2)} I_0(\phi_m r)$$

Continuity of flux and current at r_u gives a pair of equations from Equations 10 and 13 which can be solved simultaneously to give

$$\frac{A}{S_m} = \frac{D_m \phi_m M_1(\phi_m r_u)}{\Delta} \quad (14)$$

and

$$\frac{C}{S_m} = - \frac{D_u \phi_u I_1(\phi_u r_u)}{\Delta} \quad (15)$$

where

$$M_1(\phi_m r) = K_1(\phi_m r) - \frac{K_1(\phi_m r_2)}{I_1(\phi_m r_2)} I_1(\phi_m r)$$

and

$$\Delta = \sum_m \left[D_m \phi_m I_0(\phi_u r_u) M_1(\phi_m r_u) + D_u \phi_u I_1(\phi_u r_u) M_0(\phi_m r_u) \right]$$

with

$$\frac{dM_0(x)}{dx} = -M_1(x) \quad .$$

The thermal utilization, f , is the ratio of the thermal neutrons absorbed in the fuel to the total thermal neutrons absorbed. This ratio is equivalent to the ratio of the thermal neutrons absorbed in the fuel to the total thermal neutron source assuming no net leakage from the cell.

$$f = \frac{\sum_u \int_0^{r_u} \rho_u 2\pi r dr}{V_m S_m} \quad (16)$$

Combining Equation 10 and 16 into

$$f = \left(\frac{A}{S_m} \right) \frac{2\pi \sum_u}{V_m} \int_0^{r_u} I_0(\rho_u r) r dr \quad (17)$$

and solving the integral (1, p. 305) gives

$$f = \left(\frac{A}{S_m} \right) \frac{2\pi \sum_u}{V_m} \frac{r_u I_1(\rho_u r_u)}{\rho_u} \quad (18)$$

Combining Equations 14 and 18 and solving for the reciprocal of f gives

$$\frac{1}{f} = 1 + \frac{V_m \sum_m}{V_u \sum_u} F + (E - 1) \quad (19)$$

where

$$F = \frac{\rho_u r_u}{2} \frac{I_0(\rho_u r_u)}{I_1(\rho_u r_u)} \quad (20)$$

and

$$E - 1 = \left[\frac{V_m}{V_u} \frac{\rho_m r_u}{2} \frac{M_0(\rho_m r_u)}{M_1(\rho_m r_u)} \right] - 1 \quad (21)$$

(11)

$$\frac{2 + 3\sqrt{2} + 3\sqrt{2}}{2\sqrt{2}} = 2$$

Substituting the value of x in the given equation

(12)

$$2 + 3\sqrt{2} + 3\sqrt{2} = 2\sqrt{2} \left(\frac{2}{\sqrt{2}} \right) = 2$$

Substituting the value of x in the given equation

(13)

$$\frac{2 + 3\sqrt{2} + 3\sqrt{2}}{2\sqrt{2}} = 2\sqrt{2} \left(\frac{2}{\sqrt{2}} \right) = 2$$

Substituting the value of x in the given equation

Substituting the value of x in the given equation

(14)

$$(2 + 3) = 2\sqrt{2} \left(\frac{2}{\sqrt{2}} \right) = 2 + 3$$

(15)

$$\frac{2 + 3\sqrt{2} + 3\sqrt{2}}{2\sqrt{2}} = 2\sqrt{2} \left(\frac{2}{\sqrt{2}} \right) = 2$$

(16)

$$2 + 3\sqrt{2} + 3\sqrt{2} = 2\sqrt{2} \left(\frac{2}{\sqrt{2}} \right) = 2 + 3$$

F is the disadvantage factor of the uranium which is the ratio of the neutron flux at the rod surface to the average flux in the rod interior (5, p.270).

$$F = \frac{\phi_u(r_u)}{\bar{\phi}_u} \quad (22)$$

The average thermal neutron flux in the moderator is greater than the thermal neutron flux at the rod surface because the diffusion coefficient in the moderator is finite. The additional absorption is measured by the quantity $(E - 1)$, the excess absorption term.

Murray (1, p. 100) assumed that any poisons that are tolerable do not appreciably disturb the basic neutron flux distribution from that of the configuration with fuel and moderator only. Therefore, the aluminum cladding, coolant, and the process tube assembly can all be treated as poisons. The reciprocal thermal utilization with this modification can be written

$$\frac{1}{k_p} = \frac{1}{k} + \sum_{i=0}^{n \text{ poisons}} \frac{V_i \Sigma_i \bar{\phi}_i}{V_u \Sigma_u \bar{\phi}_u} \quad (23)$$

where the average neutron flux in the added poison or absorber is $\bar{\phi}_i$.

It is not immediately evident that the condition is satisfied by the functions f_1 and f_2 defined above. In fact, it is not satisfied by the functions f_1 and f_2 defined above.

$$\frac{f_1(x)}{f_2(x)}$$

The condition is satisfied by the functions f_1 and f_2 defined above. In fact, it is not satisfied by the functions f_1 and f_2 defined above. The condition is satisfied by the functions f_1 and f_2 defined above. The condition is satisfied by the functions f_1 and f_2 defined above.

The condition is satisfied by the functions f_1 and f_2 defined above. In fact, it is not satisfied by the functions f_1 and f_2 defined above. The condition is satisfied by the functions f_1 and f_2 defined above. The condition is satisfied by the functions f_1 and f_2 defined above.

$$\left\{ \frac{f_1(x)}{f_2(x)} \right\} = \frac{f_1(x)}{f_2(x)}$$

The condition is satisfied by the functions f_1 and f_2 defined above. In fact, it is not satisfied by the functions f_1 and f_2 defined above. The condition is satisfied by the functions f_1 and f_2 defined above.

Assuming that for the cladding, water annulus, and process tube the ratio $\bar{\phi}_1 / \bar{\phi}_u$ is approximately equal to $\phi_u(r_u) / \bar{\phi}_u$, Equation 23 can be solved directly. Murray (1, p. 100) suggested that a slight refinement to Equation 23 may be made by letting Σ_1 be the difference between the actual poison cross section and the moderator cross section that it physically replaces.

Littler and Raffle (10, p. 94) give a useful approximation for the excess absorption term, $E - 1$.

$$E - 1 = \frac{\sigma_a^2 r_2^2}{2} \left[\frac{r_2^2}{r_2^2 - r_1^2} \ln \frac{r_2}{r_1} - \frac{3}{4} + \frac{r_1^2}{4r_2^2} \right] \quad (24)$$

The constants used in Equation 23 were listed in Tables 1 and 2. The equivalent cell dimensions were derived from direct measurements and calculations. The thermal neutron macroscopic cross sections for aluminum (cladding), water, and graphite were calculated from Equation 25 using literature values of σ_a (1), (5), and (11).

$$\Sigma = \frac{\rho \sigma^N N_0}{A} \quad (25)$$

where N_0 is 6.02×10^{23} nuclei/mole,
and A is the mass number.

...the

... ..

... ..

... ..

$$\left[\frac{a}{b} + \frac{c}{d} \right] = \frac{ad+bc}{bd}$$

... ..

... ..

... ..

... ..

... ..

... ..

$$\frac{a}{b} = \frac{c}{d}$$

... ..

... ..

\sum_a^p for the aluminum process tube was calculated using a modification of Equation 25 to account for the alloying materials in the aluminum alloy. The maxwellian distribution correction and a "not-1/v" correction was used to determine an effective absorption cross section for natural uranium. All the macroscopic cross section values used in this theoretical analysis are shown in Table 2.

Due to the limitations of simple diffusion theory, transport theory must be used for the calculation of \mathscr{H}_u . Murray (1, p. 88) gives for the uranium fuel the relationship

$$\frac{\mathscr{H}_u}{\sum^u} = \tanh \frac{\mathscr{H}_u}{\sum^u} \quad (26)$$

where \sum^u is the total cross section.

Solving Equation 25 using cross section values from Table 2 gave a value of 0.675 cm^{-1} for \mathscr{H}_u . The inverse diffusion lengths for graphite and water were found using Equation 27 and values of the diffusion lengths from the literature (5).

$$\mathscr{H} \equiv \frac{1}{L} = (\sum_a/D)^{1/2} \quad (27)$$

The thermal utilizations for the dry lattice configurations were calculated by omitting the term for water in Equation 23. The volume ratios in Equation 19 and 23 are equivalent to area ratios.

The constants listed in Tables 1 and 2 were used in Equations 19, 20, 23, and 24 to evaluate the composite thermal utilizations for the various lattice configurations considered. A Bessel function table (12) was used to evaluate the disadvantage factor, F , in Equation 20. Equation 24 was used to evaluate the excess absorption term, $(E - 1)$.

The resulting thermal utilizations computed by Method A are listed in Table 3 for the various lattice configurations.

2. Method B

A second method of calculating the thermal utilization of uranium is the method of Rumsey and Volkoff (2), (3). This method is an extension of prior work in heterogeneous lattice theory (4), (6) and includes the moderating effect of a water annulus in the lattice cell.

$$f_u = f_0 (1 + \delta) \quad (28)$$

$$\text{where } \frac{1}{f_0} - 1 = R_{al} + R_p + R_w + R_g + S_w + S_g + B_{wp} + B_{wg} \quad (29)$$

$$\text{and } \delta = \frac{\frac{q_w V_w}{q_g V_g}}{1 + \frac{q_w V_w}{q_g V_g}} \left[(E - 1) + \frac{1}{2} \kappa_w^2 t_w^2 \frac{N_E \sigma_E V_E}{N_w \sigma_w V_w} \right] \quad (30)$$

The following table shows the results of the experiments conducted on the effect of the concentration of the solution on the rate of reaction. The results are given in the following table:

Concentration of Solution (M)	Rate of Reaction (mol/l.s)
0.1	0.001
0.2	0.002
0.3	0.003
0.4	0.004
0.5	0.005

It is seen from the above table that the rate of reaction increases with the concentration of the solution. This is due to the fact that the concentration of the solution is directly proportional to the number of molecules of the reactants per unit volume. As the concentration increases, the number of molecules per unit volume also increases, and hence the rate of reaction increases.

The following table shows the results of the experiments conducted on the effect of the temperature on the rate of reaction. The results are given in the following table:

Temperature (°C)	Rate of Reaction (mol/l.s)
20	0.001
30	0.002
40	0.004
50	0.008

It is seen from the above table that the rate of reaction increases with the temperature. This is due to the fact that the rate of reaction is directly proportional to the temperature. As the temperature increases, the rate of reaction also increases.

$$10 = 10 \times 10^{-2}$$

$$10 = 10 \times 10^{-2} = 10^{-1}$$

$$\frac{10}{10} = \frac{10}{10} = 1$$

The "relative absorption" term, R_j , denotes per thermal neutron captured in the uranium, the number of thermal neutrons which would be captured in the j th medium if the neutron density in the j th medium were uniformly equal to the neutron density at the uranium-aluminum interface.

$$R_j = \frac{N_j \sigma_j V_j}{N_u \sigma_u V_u} F = \frac{\sum_j V_j}{\sum_u V_u} \cdot F \quad (31)$$

where F is the disadvantage factor of the uranium, Equation 20.

The "self blocking" term, S_j , denotes per thermal neutron absorbed in the uranium, the excess number of thermal neutrons captured in the j th medium due to the excess density of neutrons in the j th medium over the neutron density at the $i - j$ th interface.

$$S_w = \frac{1}{2} \kappa_w^2 t_w^2 \quad (32)$$

and
$$S_g = (E - 1) \left[1 + R_{al} + R_p + R_w + B_{wp} + S_w \right] \quad (33)$$

where $(E - 1)$ is the disadvantage factor of the moderator or excess absorption term given by Equation 24.

The "blocking term", B_{ij} , denotes per thermal neutron absorbed in uranium, the excess number of thermal neutrons

captured in the j th medium due to neutron density rise across the i th medium.

$$B_{wp} = \mathcal{H}_w^2 t_w^2 \frac{N_p \sigma_p V_p}{N_w \sigma_w V_w} = \mathcal{H}_w^2 t_w^2 \frac{\sum_p V_p}{\sum_w V_w} \quad (34)$$

and

$$B_{wg} = \mathcal{H}_w^2 t_w^2 \left\{ \frac{N_g \sigma_g V_g}{N_w \sigma_w V_w} + R_g \left[\frac{1}{2} + \frac{N_{al} \sigma_{al} (V_{cap} + V_{can})}{N_w \sigma_w V_w} \right] \right\} \quad (35)$$

In the above six equations \mathcal{H}_w is the inverse diffusion length of water, and t_w is the thickness of the water annulus. The cross section values are listed in Table 2, and the volume values per slug are listed in Table 1. The value of $(\beta - 1)$ is given by Equation 24 which is an approximation of the complex Bessel function in Equation 21. The approximation is considered to be sufficiently accurate for the two lattice geometries.

The production rate of thermal neutrons per unit volume per second for water and graphite are denoted q_w and q_g respectively. The ratio of the slowing down power of water to graphite, q_w/q_g , equals 20 (3, p. 22).

Figure 1 and Figure 2 show the neutron density distribution in the dry and wet lattice configurations respectively. The several terms of the competitive absorption, Equation 29, are shown schematically in these diagrams. The placement of

Proposition 1. Let \mathcal{H} be a Hilbert space and \mathcal{A} a subalgebra of $\mathcal{B}(\mathcal{H})$. Then the following conditions are equivalent:

$$(1) \quad \mathcal{A} \text{ is a von Neumann algebra} \iff \mathcal{A}'' = \mathcal{A}$$

$$(2) \quad \mathcal{A} \text{ is a von Neumann algebra} \iff \mathcal{A} \text{ is closed in the weak operator topology}$$

Proof. (1) \Rightarrow (2). Let \mathcal{A} be a von Neumann algebra. Then \mathcal{A} is closed in the weak operator topology. Suppose $\{T_\alpha\}$ is a net in \mathcal{A} which converges weakly to T . Then T is in \mathcal{A} . (2) \Rightarrow (1). Let \mathcal{A} be a subalgebra of $\mathcal{B}(\mathcal{H})$ which is closed in the weak operator topology. Then \mathcal{A} is a von Neumann algebra.

Definition. Let \mathcal{A} be a von Neumann algebra. The commutant of \mathcal{A} is the set of all operators in $\mathcal{B}(\mathcal{H})$ which commute with every operator in \mathcal{A} . The double commutant of \mathcal{A} is the von Neumann algebra generated by \mathcal{A} .

the individual absorption terms, defined in Equations 31 through 35, and the relative magnitude of these various terms can also be seen in the diagram. Any absorption of neutrons by the air in the air annulus was neglected. The net flow of thermal neutrons across the boundary of a cell was assumed to be zero.

The terms S_{al} , S_p , B_{alw} , B_{alp} , B_{alg} , and B_{pg} which are shown in Figure 1 and Figure 2 were assumed as negligible and were not included in Equation 29. At the uranium-aluminum interface, continuity of the neutron flux density and current density was assumed. The neutron current density was also assumed as linear through the thin mediums (al, p, or w) considered.

As an example, in deriving the S_{al} term, the aluminum surface neutron flux is

$$\phi_{al}^{surface} = \phi_u(r_u) + t_{al} \left(\frac{d\phi_{al}}{dr} \right)_{r_u}$$

and with Equation (10) is

$$\phi_{al}^{surface} = \phi_u(r_u) + t_{al} \left(\frac{D_u}{D_{al}} \right) A \phi_u I_1(\phi_u r_u)$$

By definition the "self blocking" term for aluminum is

$$S_{al} = \frac{(\phi_{al}^{ave} - \phi_u^{surface})}{\phi_u^{ave}} \frac{V_{al} \sum_a^{al}}{V_u \sum_a^u} \quad (36)$$

and taking from (10, p. 89)

$$\phi_u^{ave} = \frac{2\lambda}{H_u r_u} I_1 (H_u r_u)$$

and substituting gives

$$S_{al} \approx \frac{1}{2} t_{al}^2 H_{al}^2 \quad (37)$$

Similarly

$$S_w \approx \frac{1}{2} t_w^2 H_w^2 \quad (32)$$

and

$$S_p \approx \frac{1}{2} t_p^2 H_p^2$$

A calculation of S_{al} , Equation 37, showed that with $H_{al}^2 = 0.00244 \text{ cm}^{-2}$ (10, p. 93) and $t_{al} = 0.102 \text{ cm}$, that $S_{al} = 1.27 \times 10^{-5}$. This value is of a magnitude which can be considered negligible.

The very small factor, $(H_i t_i)^2$, for the cladding and process tube causes the terms S_{al} , S_p , B_{alw} , B_{alp} , B_{alg} , and B_{pg} to become negligible with respect to the other terms in Figure 1 and Figure 2. With these eliminations, Figure 1 and Figure 2 agree with Equation 29.

$$(11) \quad \frac{\frac{1}{2} \frac{1}{2} \frac{1}{2}}{\frac{1}{2} \frac{1}{2} \frac{1}{2}} = \frac{\left(\frac{1}{2} \frac{1}{2} \frac{1}{2} \right)}{\frac{1}{2} \frac{1}{2} \frac{1}{2}} = \frac{1}{2}$$

the 1st 2nd 3rd 4th 5th 6th 7th 8th 9th 10th

$$\frac{1}{2} \frac{1}{2} \frac{1}{2} = \frac{1}{2} \frac{1}{2} \frac{1}{2}$$

the 1st 2nd 3rd 4th 5th 6th 7th 8th 9th 10th

$$(12) \quad \frac{1}{2} \frac{1}{2} \frac{1}{2} = \frac{1}{2} \frac{1}{2} \frac{1}{2}$$

the 1st 2nd 3rd 4th 5th 6th 7th 8th 9th 10th

$$(13) \quad \frac{1}{2} \frac{1}{2} \frac{1}{2} = \frac{1}{2} \frac{1}{2} \frac{1}{2}$$

$$\frac{1}{2} \frac{1}{2} \frac{1}{2} = \frac{1}{2} \frac{1}{2} \frac{1}{2}$$

the 1st 2nd 3rd 4th 5th 6th 7th 8th 9th 10th
the 1st 2nd 3rd 4th 5th 6th 7th 8th 9th 10th
the 1st 2nd 3rd 4th 5th 6th 7th 8th 9th 10th
the 1st 2nd 3rd 4th 5th 6th 7th 8th 9th 10th

the 1st 2nd 3rd 4th 5th 6th 7th 8th 9th 10th
the 1st 2nd 3rd 4th 5th 6th 7th 8th 9th 10th
the 1st 2nd 3rd 4th 5th 6th 7th 8th 9th 10th
the 1st 2nd 3rd 4th 5th 6th 7th 8th 9th 10th

The constants listed in Tables 1 and 2 were used in Equations 28 through 35 to evaluate the wet configuration thermal utilizations by the Rumsey and Volkoff method. Equation 20 was used to evaluate F in Equation 31. The value $(E - 1)$ in Equation 33 was evaluated by using Equation 24. The thermal utilizations for the dry configurations were calculated using Equations 28 through 35 with the terms for water omitted. The resulting thermal utilizations, Method B, are listed in Table 3 for the various configurations.

E. Resonance Escape Probability

The fraction of fast fission neutrons that reach thermal energy without experiencing capture while slowing down, is called the resonance escape probability, p . The methods of Murray (1) and of Rumsey and Volkoff (2) were also used to theoretically determine the resonance escape factor. These methods are considered separately and are denoted Methods A and B respectively.

1. Method A

Murray (1, p. 92) gives the heterogeneous equivalent for p as

$$p = \exp \left[- \frac{V_u \bar{\rho}_u \sum_{re}^u}{V_m \bar{\rho}_m \bar{k} \sum_s^m} \right] \quad (38)$$

where Σ_{re}^u is the effective macroscopic cross section.

The form of Equation 38 suggests a resemblance to similar ratios appearing in the expression to evaluate f .

A definition of the resonance utilization, f_r , is

$$f_r = \frac{\text{resonance absorption in fuel}}{\text{resonance absorption in fuel} + \text{scattering "absorption" by moderator}} \quad (39)$$

The resonance absorption by the uranium is $\bar{\sigma}_u v_u \Sigma_0$ from a thermal flux absorption analogy, where Σ_0 is an appropriately chosen average cross section of uranium over the entire resonance flux region.

Assuming that the flux over the resonance region is $1/E$ dependent, the average cross section is

$$\bar{\sigma}_u = \frac{\int \sigma_a^u \frac{dE}{E}}{\int \frac{dE}{E}} = \frac{\sigma_r}{\ln \frac{E_1}{E_2}} \quad (40)$$

where $\ln \frac{E_1}{E_2} = 5.6$ for uranium metal (5, p. 273). The presence of the moderator and the geometric nature of the heterogeneous lattice requires that an effective resonance integral (σ_{re}) be used for the value of σ_r . Equation 40 is then

$$\bar{\sigma}_u = \frac{\sigma_{re}^u}{5.6} \quad (41)$$

where (1, p. 93)

$$\sigma_{re}^u = \int (\sigma_{au}) \text{ eff } \frac{dE}{E} = 9.25 + 24.7 S/M \quad (42)$$

and S/M is the fuel surface to mass ratio in cm^2/g .

$$\text{Finally } \Sigma_0 = \frac{N_u \sigma_{re}^u}{5.6} = \frac{\Sigma_{re}^u}{5.6} \quad (43)$$

The scattering "absorption" by the moderator would be $\bar{\phi}_m V_m \Sigma_1^m$ from a thermal flux absorption analogy,

$$\text{where } \Sigma_1^m = \frac{\int \bar{\phi} \Sigma_s \frac{dE}{E}}{\int \frac{dE}{E}} = \frac{\bar{\phi} \Sigma_s}{5.6} \quad (44)$$

With Equations 39, 43, and 44 the magnitude of the exponent of p in Equation 38 is

$$\frac{V_u \bar{\phi}_u \Sigma_{re}^u}{V_m \bar{\phi}_m \bar{\phi} \Sigma_s^m} = \left(\frac{1}{f_r} - 1 \right)^{-1} \quad (45)$$

Murray (1, p. 94) gives an empirical expression for the effective resonance inverse diffusion length of uranium,

$$\kappa_u^{re} = 0.0222 \rho_u \text{ cm}^{-1} \quad (46)$$

where ρ_u is expressed in g/cm^3 .

(13) $\nabla \cdot \mathbf{u} = 0$ inside

(14) $\nabla \cdot (\mathbf{u} \otimes \mathbf{u}) + \nabla p = \frac{\mu}{\rho} \nabla^2 \mathbf{u}$ in Ω

where Ω is the unit ball in \mathbb{R}^n and $\mathbf{u} \cdot \mathbf{n} = 0$ on $\partial\Omega$.

(15) $\frac{\partial^2 u}{\partial x^2} + \frac{\partial^2 u}{\partial y^2} = 0$ in Ω

where Ω is the unit ball in \mathbb{R}^2 and $u = 0$ on $\partial\Omega$.

where Ω is the unit ball in \mathbb{R}^n and $u = 0$ on $\partial\Omega$.

(16) $\frac{\partial^2 u}{\partial x^2} + \frac{\partial^2 u}{\partial y^2} = 0$ in Ω

where Ω is the unit ball in \mathbb{R}^2 and $u = 0$ on $\partial\Omega$.

(17) $\frac{\partial^2 u}{\partial x^2} + \frac{\partial^2 u}{\partial y^2} = 0$ in Ω

where Ω is the unit ball in \mathbb{R}^2 and $u = 0$ on $\partial\Omega$.

(18) $\frac{\partial^2 u}{\partial x^2} + \frac{\partial^2 u}{\partial y^2} = 0$ in Ω

where Ω is the unit ball in \mathbb{R}^2 and $u = 0$ on $\partial\Omega$.

The effective resonance inverse diffusion length for graphite is,

$$\kappa_g^{re} = \sqrt{3 \sum_1^m \sum_t^g} \quad (47)$$

where \sum_t^g is the actual transport cross section of the graphite averaged over the entire resonance flux region. To evaluate \sum_t^g , the relationship

$$\sum_t^g = \sum_s^g (1 - \overline{\cos \theta}) \quad (48)$$

is derived from (5, p. 98)

$$\lambda_t = \lambda_s / (1 - \overline{\cos \theta}) \quad (49)$$

$$\text{where } \overline{\cos \theta} = 2/3A \quad (50)$$

and A is the moderator mass number.

The method of calculating f is now borrowed to find f_r . Equation 19 modified is

$$\frac{1}{f_r} = 1 + \frac{V_g}{V_u} \frac{\sum_1^m}{\sum_0} P + (E - 1) \quad (51)$$

The values of κ_u^{re} and κ_g^{re} were determined from Equations 46 and 47. \sum_0 and \sum_1^m were calculated from Equations 43 and 44.

The following is a list of the numbers 1 through 1000.

1000 999 998 997 996 995 994 993 992 991 990 989 988 987 986 985 984 983 982 981 980 979 978 977 976 975 974 973 972 971 970 969 968 967 966 965 964 963 962 961 960 959 958 957 956 955 954 953 952 951 950 949 948 947 946 945 944 943 942 941 940 939 938 937 936 935 934 933 932 931 930 929 928 927 926 925 924 923 922 921 920 919 918 917 916 915 914 913 912 911 910 909 908 907 906 905 904 903 902 901 900 899 898 897 896 895 894 893 892 891 890 889 888 887 886 885 884 883 882 881 880 879 878 877 876 875 874 873 872 871 870 869 868 867 866 865 864 863 862 861 860 859 858 857 856 855 854 853 852 851 850 849 848 847 846 845 844 843 842 841 840 839 838 837 836 835 834 833 832 831 830 829 828 827 826 825 824 823 822 821 820 819 818 817 816 815 814 813 812 811 810 809 808 807 806 805 804 803 802 801 800 799 798 797 796 795 794 793 792 791 790 789 788 787 786 785 784 783 782 781 780 779 778 777 776 775 774 773 772 771 770 769 768 767 766 765 764 763 762 761 760 759 758 757 756 755 754 753 752 751 750 749 748 747 746 745 744 743 742 741 740 739 738 737 736 735 734 733 732 731 730 729 728 727 726 725 724 723 722 721 720 719 718 717 716 715 714 713 712 711 710 709 708 707 706 705 704 703 702 701 700 699 698 697 696 695 694 693 692 691 690 689 688 687 686 685 684 683 682 681 680 679 678 677 676 675 674 673 672 671 670 669 668 667 666 665 664 663 662 661 660 659 658 657 656 655 654 653 652 651 650 649 648 647 646 645 644 643 642 641 640 639 638 637 636 635 634 633 632 631 630 629 628 627 626 625 624 623 622 621 620 619 618 617 616 615 614 613 612 611 610 609 608 607 606 605 604 603 602 601 600 599 598 597 596 595 594 593 592 591 590 589 588 587 586 585 584 583 582 581 580 579 578 577 576 575 574 573 572 571 570 569 568 567 566 565 564 563 562 561 560 559 558 557 556 555 554 553 552 551 550 549 548 547 546 545 544 543 542 541 540 539 538 537 536 535 534 533 532 531 530 529 528 527 526 525 524 523 522 521 520 519 518 517 516 515 514 513 512 511 510 509 508 507 506 505 504 503 502 501 500 499 498 497 496 495 494 493 492 491 490 489 488 487 486 485 484 483 482 481 480 479 478 477 476 475 474 473 472 471 470 469 468 467 466 465 464 463 462 461 460 459 458 457 456 455 454 453 452 451 450 449 448 447 446 445 444 443 442 441 440 439 438 437 436 435 434 433 432 431 430 429 428 427 426 425 424 423 422 421 420 419 418 417 416 415 414 413 412 411 410 409 408 407 406 405 404 403 402 401 400 399 398 397 396 395 394 393 392 391 390 389 388 387 386 385 384 383 382 381 380 379 378 377 376 375 374 373 372 371 370 369 368 367 366 365 364 363 362 361 360 359 358 357 356 355 354 353 352 351 350 349 348 347 346 345 344 343 342 341 340 339 338 337 336 335 334 333 332 331 330 329 328 327 326 325 324 323 322 321 320 319 318 317 316 315 314 313 312 311 310 309 308 307 306 305 304 303 302 301 300 299 298 297 296 295 294 293 292 291 290 289 288 287 286 285 284 283 282 281 280 279 278 277 276 275 274 273 272 271 270 269 268 267 266 265 264 263 262 261 260 259 258 257 256 255 254 253 252 251 250 249 248 247 246 245 244 243 242 241 240 239 238 237 236 235 234 233 232 231 230 229 228 227 226 225 224 223 222 221 220 219 218 217 216 215 214 213 212 211 210 209 208 207 206 205 204 203 202 201 200 199 198 197 196 195 194 193 192 191 190 189 188 187 186 185 184 183 182 181 180 179 178 177 176 175 174 173 172 171 170 169 168 167 166 165 164 163 162 161 160 159 158 157 156 155 154 153 152 151 150 149 148 147 146 145 144 143 142 141 140 139 138 137 136 135 134 133 132 131 130 129 128 127 126 125 124 123 122 121 120 119 118 117 116 115 114 113 112 111 110 109 108 107 106 105 104 103 102 101 100 99 98 97 96 95 94 93 92 91 90 89 88 87 86 85 84 83 82 81 80 79 78 77 76 75 74 73 72 71 70 69 68 67 66 65 64 63 62 61 60 59 58 57 56 55 54 53 52 51 50 49 48 47 46 45 44 43 42 41 40 39 38 37 36 35 34 33 32 31 30 29 28 27 26 25 24 23 22 21 20 19 18 17 16 15 14 13 12 11 10 9 8 7 6 5 4 3 2 1

$$(14) \quad \sqrt[3]{3^3 3^3} = 3^2$$

When the cube root of 3 is taken, the result is $\sqrt[3]{3}$. When the cube root of 3 is taken again, the result is $\sqrt[3]{\sqrt[3]{3}}$. When the cube root of 3 is taken a third time, the result is $\sqrt[3]{\sqrt[3]{\sqrt[3]{3}}}$.

$$(15) \quad \sqrt[3]{3^3} = 3$$

When the cube root of 3 is taken, the result is $\sqrt[3]{3}$.

$$(16) \quad \sqrt[3]{3^3} = 3$$

$$(17) \quad \sqrt[3]{3^3} = 3$$

When the cube root of 3 is taken, the result is $\sqrt[3]{3}$.

When the cube root of 3 is taken again, the result is $\sqrt[3]{\sqrt[3]{3}}$. When the cube root of 3 is taken a third time, the result is $\sqrt[3]{\sqrt[3]{\sqrt[3]{3}}}$.

$$(18) \quad \sqrt[3]{3^3} = 3$$

When the cube root of 3 is taken, the result is $\sqrt[3]{3}$. When the cube root of 3 is taken again, the result is $\sqrt[3]{\sqrt[3]{3}}$. When the cube root of 3 is taken a third time, the result is $\sqrt[3]{\sqrt[3]{\sqrt[3]{3}}}$.

Using the above values of κ_u^{re} and κ_g^{re} , F was determined from Equation 20 and $(E - 1)$ was determined from Equation 24. Table 2 lists all the important lattice material constants.

Solving Equation 51 and using the value of f_r in Equation 45 determined the exponent of p in Equation 38. The resonance escape probabilities for the various configurations, Method A, are listed in Table 3. The values of p for the wet and dry configurations were the same using Method A.

2. Method B

Volkoff and Rumsey (2, p. 293) express the equation for the resonance escape probability as

$$p = \exp \left[- \frac{f_r}{1 - f_r} \right] \quad (52)$$

where f_r is the resonance utilization of uranium for resonance neutrons. Noting the form similarity of the exponent of Equation 52 to the thermal utilization equations, the factor, f_r , is

$$f_r = f_0 (1 + \delta) \quad (53)$$

with

$$\frac{1}{f_0} - 1 = R_{al} + R_p + R_w + R_g + S_w + S_g + B_{wp} + B_{wg} \quad (54)$$

changing the cross sections Σ_a^u to Σ_0 and Σ_a^g to Σ_1^m in Equations 31, 33, and 35 gives a solution to Equation 54.

δ is given by Equation 30.

Substituting the individual terms in Equation 54 gives

$$\frac{1}{F_0} - 1 = Z + Y \quad (55)$$

where

$$Z = \frac{F}{\Sigma_0 V_u} \left\{ \Sigma_1^m V_g \left[1 + \mu_w^2 t_w^2 \left(\frac{1}{2} + \frac{\Sigma_{al} V_{cap} + can}{\Sigma_w V_w} \right) \right] + (E) \left(\Sigma_{al} V_{al} + \Sigma_p V_p + \Sigma_w V_w \right) \right\} \quad (56)$$

and

$$Y = \mu_w^2 t_w^2 \left\{ \frac{1}{\Sigma_w V_w} \left[(E) \Sigma_p V_p + \Sigma_1^m V_g \right] + \frac{E}{2} \right\} + (E - 1) \quad (57)$$

Combining Equations 52, 53, and 55 gives

$$p = \exp \left[- \frac{(1 + \delta)}{Z + Y - \delta} \right] \quad (58)$$

The value of E was again obtained from Equation 24. The average cross section of uranium over the resonance region, Σ_0 , is given by Equation 43. The scattering "absorption" cross section of the moderator over the resonance region, Σ_1^m , is given by Equation 44. Using values from Tables 1 and 2

Let \mathcal{S} be a set of n elements. Let \mathcal{S}' be a set of n' elements.

Let \mathcal{S}'' be a set of n'' elements. Let \mathcal{S}''' be a set of n''' elements.

Let $\mathcal{S}^{(4)}$ be a set of $n^{(4)}$ elements. Let $\mathcal{S}^{(5)}$ be a set of $n^{(5)}$ elements.

Let $\mathcal{S}^{(6)}$ be a set of $n^{(6)}$ elements. Let $\mathcal{S}^{(7)}$ be a set of $n^{(7)}$ elements.

$$(10) \quad \mathcal{S}^{(8)} = \mathcal{S}^{(7)} \cup \mathcal{S}^{(6)}$$

$$(11) \quad \left\{ \left(\frac{n^{(8)} + n^{(7)} + n^{(6)}}{n^{(8)}} \right) \mathcal{S}^{(8)} \right\} \frac{n^{(8)}}{n^{(8)}} = n^{(8)}$$

$$(12) \quad \left\{ \mathcal{S}^{(8)} \cup \mathcal{S}^{(7)} \cup \mathcal{S}^{(6)} \right\} \frac{n^{(8)}}{n^{(8)}} = n^{(8)}$$

$$(13) \quad \left\{ \frac{n^{(8)}}{n^{(8)}} \left(\mathcal{S}^{(8)} \cup \mathcal{S}^{(7)} \cup \mathcal{S}^{(6)} \right) \right\} \frac{n^{(8)}}{n^{(8)}} = n^{(8)}$$

Let $\mathcal{S}^{(9)}$ be a set of $n^{(9)}$ elements. Let $\mathcal{S}^{(10)}$ be a set of $n^{(10)}$ elements.

$$(14) \quad \left[\frac{n^{(9)} + n^{(10)}}{n^{(9)}} \right] \mathcal{S}^{(9)} = n^{(9)}$$

Let $\mathcal{S}^{(11)}$ be a set of $n^{(11)}$ elements. Let $\mathcal{S}^{(12)}$ be a set of $n^{(12)}$ elements.

Let $\mathcal{S}^{(13)}$ be a set of $n^{(13)}$ elements. Let $\mathcal{S}^{(14)}$ be a set of $n^{(14)}$ elements.

Let $\mathcal{S}^{(15)}$ be a set of $n^{(15)}$ elements. Let $\mathcal{S}^{(16)}$ be a set of $n^{(16)}$ elements.

$$(15) \quad \mathcal{S}^{(17)} = \mathcal{S}^{(16)} \cup \mathcal{S}^{(15)}$$

Let $\mathcal{S}^{(18)}$ be a set of $n^{(18)}$ elements. Let $\mathcal{S}^{(19)}$ be a set of $n^{(19)}$ elements.

and Equations 20, 24, 30, 43, 44, 46, 47, 56, 57, and 58 the resonance escape probability was determined for Method B. These values of p are listed in Table 3 for the lattice configurations considered. The dry values for p were obtained by eliminating the terms for water in all equations.

F. Buckling

The theoretical buckling was computed using Equations 1 and 2. The diffusion length for each lattice configuration was calculated by (5, p. 280)

$$L^2 = \frac{D}{\Sigma_a} = L_g^2(1 - f) \quad (59)$$

where L_g is the diffusion length in pure moderator. The value of f used in each case was the theoretically determined value listed in Table 3. The Fermi age, τ , of the thermal neutrons for the lattice configurations was assumed to be the same as τ for the moderator. Murray (1, p. 123) gives the value of τ as 364 cm^2 . The value of k_∞ for each configuration was determined from the values of ϵ , η , f , and p listed in Table 3 for each configuration.

The volume of a cubical critical reactor having the given lattice configuration is

$$V_T = \frac{161}{B_g^3} \quad (60)$$

The square of the lattice diffusion length and the buckling for each of the lattice configurations considered are listed in Table 4. The volume and cube side length of a cubical critical reactor for each considered lattice configuration are also listed in Table 4.

The history of the United States is a story of the struggle for freedom and justice for all. It is a story of the brave men and women who have fought for the principles of liberty and equality. It is a story of the triumph of the human spirit over adversity and oppression. It is a story that inspires us to strive for a better world for ourselves and for future generations.

The United States is a land of opportunity and hope. It is a land where every person has the right to pursue the American dream. It is a land where diversity is celebrated and where the voices of all are heard. It is a land that has the power to change the world and to create a more just and equitable society.

The United States is a land of innovation and progress. It is a land where new ideas are born and where the frontiers of knowledge are expanded. It is a land that has led the world in many fields of science, technology, and culture. It is a land that has the potential to solve the world's most pressing problems and to create a more sustainable future.

The United States is a land of freedom and democracy. It is a land where the principles of the Constitution are upheld and where the rights of all citizens are protected. It is a land that has the power to lead the world in the pursuit of peace and justice. It is a land that has the potential to create a more just and equitable world for all.

IV. EXPERIMENTAL INVESTIGATION

A. Description of Equipment

A picture of the subcritical assembly with a 8.5 in. lattice spacing is shown in Figure 3. The physical dimensions of the graphite assembly were 60 in. x 60 in. x 79 in. The actual graphite used in the construction of the assembly was originally 7 in. diameter solid graphite rods. These rods were squared off to a 6 in. x 6 in. cross section (3.5 in. radius on the corners) and stacked as shown in Figure 3. The top five rows of the graphite rods in the assembly were 5 in. x 6 in., and the bottom nine rows were 6 in. x 6 in.

The density of the graphite was determined from a weight and dimension measurement of a mass of graphite. The graphite density was found to be 1.56 g/cm^3 .

The graphite assembly was covered on the top and four sides with a 10 mil sheet of cadmium sandwiched between a 0.375 in. thickness of plywood and 0.125 in. of masonite. The cadmium sheet gave an effective "black wall" for thermal neutrons. Adding a 0.25 in. total spacing allowance for the graphite rods a horizontal section between the "black walls" of the assembly was 60.5 in. x 60.5 in. in area. The assembly was mounted on a concrete base, and tanks of water were placed under the graphite structure to insure that adequate

THE UNIVERSITY OF CHICAGO

THE UNIVERSITY OF CHICAGO

The University of Chicago is a private research university located in Chicago, Illinois. It was founded in 1837 and is one of the oldest and most prestigious universities in the United States. The university is known for its commitment to academic excellence and its diverse range of programs and research. It has a long history of producing leaders in various fields, including science, literature, and public service. The university's campus is located in the Hyde Park neighborhood of Chicago, and it is home to some of the most famous buildings in the city. The University of Chicago is a member of the Association of American Universities and is ranked among the top universities in the world by various international ranking agencies. It is a research-intensive institution, with a strong emphasis on graduate education and the production of new knowledge. The university's faculty includes many of the most prominent scholars in their fields, and it is a hub for cutting-edge research. The University of Chicago is also known for its commitment to social justice and public engagement. It has a long history of advocating for the rights of marginalized groups and promoting social reform. The university's commitment to these values is reflected in its policies and programs, and it continues to be a leader in these areas today.

shielding was effected with the neutron source in place.

Figure 3 shows the relative placement of these tanks.

The lattice spacing was varied by changing the arrangement of the uranium filled process tubes in the assembly. The 6 in. lattice, Lattice I, was the configuration with all the lattice holes filled with process tubes. The 8.5 in. lattice, Lattice II, was the configuration as shown on Figure 3. By removing alternate rows of the process tubes from the 8.5 in. lattice, the 12 in. lattice, Lattice III, was realized.

Five plutonium-beryllium neutron sources contained in individual right cylindrical containers were placed under the center of the graphite assembly. Each of these sources emitted approximately 1.63×10^6 neutrons per second; therefore the total source strength was approximately 8.15×10^6 neutrons per second. A cruciform geometry was chosen for the placement of the five sources. One source was at each of the cruciform ends, and one was placed at the cruciform center. The total source was in this way effectively contained in a circle of about 3.5 in. in diameter.

The cylindrical uranium slugs were 1.080 in. in diameter and 8.40 in. in length. Assuming a 40 mil cladding and a 200 mil slug end cap of 2S aluminum, the actual uranium fuel size was a rod 1.00 in. in diameter and 8.00 in. in length. The density of the uranium was determined from the weights

attention was attracted to the various forms of plants

which the various plants of the same family

The various plants of the same family are

and in the various plants of the same family

and in the various plants of the same family

and in the various plants of the same family

and in the various plants of the same family

and in the various plants of the same family

and in the various plants of the same family

and in the various plants of the same family

and in the various plants of the same family

and in the various plants of the same family

and in the various plants of the same family

and in the various plants of the same family

and in the various plants of the same family

and in the various plants of the same family

and in the various plants of the same family

and in the various plants of the same family

and in the various plants of the same family

and in the various plants of the same family

and in the various plants of the same family

and in the various plants of the same family

and in the various plants of the same family

and in the various plants of the same family

and in the various plants of the same family

and dimensions of several random sample slugs. The density of natural uranium determined in this way was 19.0 g/cm^3 .

The smallest lattice spacing investigated, the 6 in. lattice, required 117 sections of 6061-T6 (commercial designation 618) aluminum tubing. The tubing sections had an outer diameter of 1.375 in., a wall thickness of 35 mils, and a length of 62 in. The composition of 618 aluminum is 0.25% copper, 0.60% silicon, 1.00% magnesium, 0.25% chromium, and the remainder aluminum.

The spacing wire composition was 28 aluminum and had a 0.102 in. diameter. The wire was used to center the uranium slugs in the process tube. Seven uranium slugs were loaded in each tube with a helical wrapping of wire around the slugs for spacing in the tube. Approximately 10 feet of wire was used for each seven slugs.

Figure 4 shows a scale drawing of an actual unit cell of the subcritical assembly with a loaded process tube in place. Number seven rubber stoppers were used at both ends of the process tubing to contain the water coolant. The stoppers were also used for the dry configurations to help contain the uranium slugs during handling of the loaded process tubes. Allowing two process tube lengths of wire for each tube, the effective thickness of the process tube was calculated to be 40 mils. The effective thickness of the water annulus was then found to be 0.107 in.

Indium foils were mounted on flat aluminum plates which in turn were placed on an aluminum holder. The holder was designed so that the depth of penetration of each foil into the slots in the assembly could be accurately determined. The indium foils were 1.5 in. x 1.0 in. x 0.003 in. and had an average weight of 0.5943 grams. The average thickness of these foils was 6.14 mg/cm^2 . Figure 5 shows the foil holder and foil placement during counting. The geometry of the foil with respect to the glass wall counting tube was held constant by use of the counter shelf holder shown in Figure 5.

A model 181A scaler manufactured by Nuclear-Chicago and a glass wall Gieger tube were used to count the beta activity of the irradiated indium foils. A conventional stop watch was used for the timing of the counting period.

B. Procedure

The uranium filled process tubes were loaded into the graphite assembly in varying arrangements for the three geometric lattices investigated. The annulus between the slug and the tube wall was filled with water for the wet configurations.

The neutron flux distribution was determined by the indium foil activation method. By determining the activity of a

The first thing I noticed when I stepped out of the car was the
 smell of the sea. It was a fresh, salty smell that I had never
 experienced before. I had been told that the air in the
 south was different, but I didn't realize how different it would be.
 The humidity was not sticky, it was welcoming. It felt like a warm
 blanket. I had heard that the humidity was bad, but in the south,
 it was perfect. It was just what I needed. I had been so
 stressed in the north, and here, in the south, I felt like I had
 found a new home. The humidity was not a curse, it was a blessing.
 It was the only thing that made me feel like I had finally
 found a place where I belonged. The humidity was not a curse,
 it was a blessing. It was the only thing that made me feel like I
 had finally found a place where I belonged.

The humidity was not a curse, it was a blessing. It was the only
 thing that made me feel like I had finally found a place where I
 belonged. The humidity was not a curse, it was a blessing. It was
 the only thing that made me feel like I had finally found a place
 where I belonged.

CHAPTER 2

The humidity was not a curse, it was a blessing. It was the only
 thing that made me feel like I had finally found a place where I
 belonged. The humidity was not a curse, it was a blessing. It was
 the only thing that made me feel like I had finally found a place
 where I belonged.

foil after a long period of irradiation and making an allowance for decay during the process of counting, the saturation activity for a given indium foil was obtained.

$$A_{\infty} = A_t e^{\lambda t} \quad (61)$$

where A_{∞} is the saturation activity,

A_t is the activity at time t ,

λ is the decay constant for indium,

and t is the time after removal from the neutron flux.

The saturation activity is proportional to the neutron flux at an equilibrium state. The irradiation time of the indium foils for each run was in all cases at least 6.5 hours. This length of time corresponds to more than seven half-lives of indium as the half life for indium is 54 minutes. The indium foils used were not exactly all the same size and weight, and therefore a normalizing correction was made. Dividing the saturation activity for a given foil by its weight resulted in a normalized saturation activity. Since a constant geometry was maintained in the counter, this operation put all of the individual foil activities on the same basis. This normalized saturation activity is the activity which is tabulated in the Appendix, Table 5 through Table 10, for all of the foil positions in each of the lattice configurations investigated.

Upon removing a foil, a three minute minimum decay time was given to each foil before beginning the count. This period of time eliminated any short lived decay components in the activated indium. All of the counts taken of the indium foils were three minutes in duration. The decay time was taken as the difference between the time of the foil's removal from the neutron flux and the mid-time of the count duration.

The foil holder slot positions on the front face of the subcritical assembly are shown on Figure 6. The horizontal x direction spacing was given letter designations A through J. The vertical z direction spacing was numbered vertically 1 through 13. The actual distance in in. from the east face was the horizontal y direction distance designation. The unit of spacing was 6 in. in all cases with the sole exception of a vertical spacing change to 5 in. at the position where the lattice structure changed to a 5 in. x 6 in. area.

A glass wall Gieger tube operating at 950 volts was used for all of the foil activity determinations. Before and after each series of runs, an operational check on the tube and scaler was made with a sample of radioactive strontium. The background activity remained essentially constant at an average of 44 counts per minute during the series of counting runs. Dead time corrections were significant only on a few of the higher counts.

The surveys taken of the various lattice configurations were as follows:

Lattices I and II, wet and dry cases.

- a. Vertical at $x = 27$ in.; $y = 18$ in. and $y = 30$ in.
- b. Horizontal, x direction, at $y = 18$ in. and $y = 30$ in.; $z = 30$ in.
- c. Horizontal, y direction, at $x = 27$ in.; $z = 30$ in.

Lattice III, wet and dry cases.

- a. Vertical at $x = 27$ in.; $y = 30$ in.

Lattice without uranium.

- a. Vertical and horizontal, x direction, at $y = 30$ in.
- b. Horizontal, y direction, at $x = 27$ in.; $z = 30$ in.

Figure 6 is a diagram showing the foil positions.

Glasstone (5, p. 284) shows that the flux variation in the vertical direction at distances not too near the top of a rectangular subcritical assembly shape is

$$\phi(z) = Ce^{-\gamma z} \quad (62)$$

with

$$\gamma^2 = \left(\frac{\pi}{a}\right)^2 + \left(\frac{\pi}{b}\right)^2 - B_m^2 \quad (63)$$

The second part of the article is devoted to the study of the asymptotic behavior of the solutions of the system (1) for large values of t . It is shown that the solutions of the system (1) are bounded for all $t \geq 0$ and that they tend to zero as $t \rightarrow \infty$. The proof of this theorem is based on the construction of a Lyapunov function. The third part of the article is devoted to the study of the asymptotic behavior of the solutions of the system (1) for large values of t . It is shown that the solutions of the system (1) are bounded for all $t \geq 0$ and that they tend to zero as $t \rightarrow \infty$. The proof of this theorem is based on the construction of a Lyapunov function. The fourth part of the article is devoted to the study of the asymptotic behavior of the solutions of the system (1) for large values of t . It is shown that the solutions of the system (1) are bounded for all $t \geq 0$ and that they tend to zero as $t \rightarrow \infty$. The proof of this theorem is based on the construction of a Lyapunov function. The fifth part of the article is devoted to the study of the asymptotic behavior of the solutions of the system (1) for large values of t . It is shown that the solutions of the system (1) are bounded for all $t \geq 0$ and that they tend to zero as $t \rightarrow \infty$. The proof of this theorem is based on the construction of a Lyapunov function. The sixth part of the article is devoted to the study of the asymptotic behavior of the solutions of the system (1) for large values of t . It is shown that the solutions of the system (1) are bounded for all $t \geq 0$ and that they tend to zero as $t \rightarrow \infty$. The proof of this theorem is based on the construction of a Lyapunov function. The seventh part of the article is devoted to the study of the asymptotic behavior of the solutions of the system (1) for large values of t . It is shown that the solutions of the system (1) are bounded for all $t \geq 0$ and that they tend to zero as $t \rightarrow \infty$. The proof of this theorem is based on the construction of a Lyapunov function. The eighth part of the article is devoted to the study of the asymptotic behavior of the solutions of the system (1) for large values of t . It is shown that the solutions of the system (1) are bounded for all $t \geq 0$ and that they tend to zero as $t \rightarrow \infty$. The proof of this theorem is based on the construction of a Lyapunov function. The ninth part of the article is devoted to the study of the asymptotic behavior of the solutions of the system (1) for large values of t . It is shown that the solutions of the system (1) are bounded for all $t \geq 0$ and that they tend to zero as $t \rightarrow \infty$. The proof of this theorem is based on the construction of a Lyapunov function. The tenth part of the article is devoted to the study of the asymptotic behavior of the solutions of the system (1) for large values of t . It is shown that the solutions of the system (1) are bounded for all $t \geq 0$ and that they tend to zero as $t \rightarrow \infty$. The proof of this theorem is based on the construction of a Lyapunov function.

$$y(t) = \begin{pmatrix} y_1(t) \\ y_2(t) \end{pmatrix}, \quad z(t) = \begin{pmatrix} z_1(t) \\ z_2(t) \end{pmatrix}$$

$$y(t) = \begin{pmatrix} y_1(t) \\ y_2(t) \end{pmatrix}, \quad z(t) = \begin{pmatrix} z_1(t) \\ z_2(t) \end{pmatrix}$$

The term B_m^2 is designated as the material buckling. The dimensions of a critical reactor can be obtained by setting $B_m^2 = B_g^2$, the geometric buckling. With the material buckling equal to the geometric buckling, B^2 is defined as the buckling. The base dimensions a and b include the extrapolation length. At large distances from the assumed source plane the harmonic corrections are assumed to be negligible.

As the neutron flux is proportional to the indium foil saturation activity, a linear plot of the logarithm of $\phi(z)$ versus the vertical position z yielded the quantity $-\gamma$ which is the slope of this plot. The base dimensions were equal in the assembly used in this investigation. By adding an extrapolation length of $0.71 \lambda_t$ to each side of the effective neutron "black wall", the square base dimensions became 62 in. Equation 63 can now be rewritten as

$$B^2 = 2 \left(\frac{\pi}{a} \right)^2 - \gamma^2 = 795 \times 10^{-6} - \gamma^2 \quad (64)$$

where the units of B^2 are cm^{-2} .

Equation 64 was used to evaluate the buckling for the wet and dry cases of all lattice geometries considered. The slope, $-\gamma$, was measured from the $x = 27$ in. and $y = 30$ in. positions of the vertical survey plots of each configuration.

V. RESULTS

The saturation activities for given foil positions of the configurations considered are tabulated in Tables 6 through 10 of the Appendix. Plots of these values, Figure 7 through Figure 16, show the vertical and horizontal distribution of the neutron flux in the subcritical assembly for the lattice configurations investigated.

The theoretical and the experimental values of the buckling and critical reactor size for the various lattice configurations considered are listed in Table 4. Figure 17 shows the relationship between the theoretical and experimental buckling values for the wet and dry cases and the lattice spacing.

The $y = 30$ in. position of the vertical flux survey plots was used for the experimental determination of buckling. The vertical flux distribution in the z direction for the $y = 18$ in. position, Figure 7 and Figure 9, was plotted only to show that the flux variation at this position was also exponential in nature. Due to the critical nature of the slope of these vertical flux plots with respect to the buckling value, the buckling from the $y = 18$ in. position was not calculated. The buckling, Equation 64, is a function of the square of the slope, $- \lambda$. Therefore a very small change in the quantity $- \lambda$ reflects a much larger change in the value of buckling.

A deviation from a true exponential nature was noted in the vertical flux plots at the lower and higher end positions of all surveys in the z direction. The lower end deviation was due to excess fast neutrons, 5 to 12 Mev, from the plutonium-beryllium neutron source. All of the neutrons from the source in this lower portion of the assembly had not as yet been moderated. The neutron absorption reaction in indium is for neutrons below 1.5 electron volts. The higher end deviation occurred approximately at the 59 in. height. This is the point where the lattice spacing changes for the three different geometric lattices considered due to the construction of the assembly. The slope of the flux plots increased near this general position in all of the vertical survey plots. Statistical error in counting the small amount of activity at high z positions accounted for the relative increase in the dispersion of the counts at these positions. These effects can be observed on the plots shown on Figure 7 through Figure 11.

The vertical flux for the wet configuration was greater than the vertical flux for the dry configuration up to $z = 36$ in. for Lattice I, Figure 7, at the $y = 18$ in. position. A similar situation existed for Lattice I, Figure 8, at the $y = 30$ in. position with the cross over at $z = 50$ in.

Figure 9 shows that the wet-dry cross over point of the flux plot for Lattice II at $y = 18$ in. occurred at $z = 30$ in. Similarly again, the wet-dry cross over point of the vertical

flux distribution plot at $y = 30$ in. for Lattice II, Figure 10, and Lattice III, Figure 11, occurred at $z = 42$ in. and $z = 38$ in. respectively. The effect of the moderation of the water was greater than the effect of the water absorption for approximately the lower half of the subcritical assembly in all lattices investigated. The water moderation effect increased the thermal neutron flux by slowing up the fast neutrons. In the lower portions of the assembly, these fast neutrons are primarily from the source. This moderation effect by the water in the process tubes was more pronounced at the $y = 30$ in. position than at the $y = 18$ in. position due to the base center position of the source. Over the center, $y = 30$ in., the neutron flux consisted of more fast neutrons at a given low horizontal plane than other positions further off center. This excess of fast neutrons was moderated in part by the water. At the $y = 18$ in. position a water moderation effect was also experienced by the fast neutrons, but the greater graphite moderation due to the greater distance from the source caused the number of fast neutrons to be smaller than at the center positions. The number of fast neutrons due to fission was also larger at the center positions than at the outer positions of the assembly. This is due to the sine distribution of the thermal neutron flux in a horizontal plane in the assembly. Thermal neutrons caused the fissions in the natural uranium which produced fast neutrons and other fission products. The position of the maximum

thermal neutron flux was therefore also the position of the maximum fast neutron flux due to fission.

The vertical flux survey for the case of the graphite lattice without uranium is shown on Figure 12. The dry configuration flux values for Lattices I, II, and III were cross plotted to indicate the cross over point on the flux plot without uranium. The flux plot of Lattice III crossed the no uranium lattice plot at a slightly higher point than the flux plot of Lattice II did. The flux of Lattice I had the lowest cross over point of the three lattices. The increase of neutron flux due to subcritical multiplication in Lattice I appeared to be less than the absorption effect of the uranium. This effect was not nearly so pronounced in Lattices II and III. The neutron flux plot for the no uranium lattice appeared to be truly exponential in character for all but the low and high extreme positions in the assembly.

The slopes of the vertical flux plots for the $x = 27$ in. and $y = 30$ in. position were determined, and it was found that the magnitude of these slopes varied as follows: the flux plot in Lattice II had the smallest slope and the flux plot in Lattice III had the greatest slope. The slope of the flux plot in Lattice I was slightly greater than the Lattice III slope. The greater the slope of the flux plot, the smaller the value of the buckling becomes. This slope variation was true for both the wet and dry configurations and was directly reflected in the buckling values calculated.

the same way as the other two, but the first is the only one that is not a

single word, and the other two are single words.

The first word is "the" and the second is "the" and the third is "the".

The first word is "the" and the second is "the" and the third is "the".

The first word is "the" and the second is "the" and the third is "the".

The first word is "the" and the second is "the" and the third is "the".

The first word is "the" and the second is "the" and the third is "the".

The first word is "the" and the second is "the" and the third is "the".

The first word is "the" and the second is "the" and the third is "the".

The first word is "the" and the second is "the" and the third is "the".

The first word is "the" and the second is "the" and the third is "the".

The first word is "the" and the second is "the" and the third is "the".

The first word is "the" and the second is "the" and the third is "the".

The first word is "the" and the second is "the" and the third is "the".

The first word is "the" and the second is "the" and the third is "the".

The first word is "the" and the second is "the" and the third is "the".

The first word is "the" and the second is "the" and the third is "the".

The first word is "the" and the second is "the" and the third is "the".

The first word is "the" and the second is "the" and the third is "the".

The first word is "the" and the second is "the" and the third is "the".

The first word is "the" and the second is "the" and the third is "the".

The first word is "the" and the second is "the" and the third is "the".

The first word is "the" and the second is "the" and the third is "the".

The first word is "the" and the second is "the" and the third is "the".

The first word is "the" and the second is "the" and the third is "the".

The first word is "the" and the second is "the" and the third is "the".

There was little difference in the effect of subcritical multiplication between the dry cases of Lattice II and III. From a vertical height of 45 in. and upwards, the flux in dry Lattice II was slightly higher than in dry Lattice III. The absorption difference in these two lattices was apparently small.

The horizontal surveys for symmetry in the x direction for $z = 30$ in. are plotted in Figure 13 through Figure 15. An extrapolation length was added to each end beyond the effective neutron "black wall". All of the symmetry plots were plotted as sine curves.

The horizontal x direction Lattice I flux, Figure 13, for the wet case was greater than the flux for the dry case at both $y = 18$ in. and $y = 30$ in. positions. The horizontal x direction Lattice II flux, Figure 13, showed that there was very little difference between the wet and the dry cases for either the $y = 18$ in. or $y = 30$ in. positions. The $y = 30$ in. position flux for both lattices was greater in magnitude than the $y = 18$ in. position flux due to the sine distribution in the y direction.

The effect of the water moderation appeared to be greater than the water absorption effect in Lattice I at both the $y = 18$ in. and $y = 30$ in. positions for the x direction survey. In the x direction survey for Lattice II, these effects were approximately equal for both y positions.

Lattice II flux in the x direction at $z = 30$ in. had in all cases almost an ideal sine distribution. The flux in wet Lattice I had some random scatter over the center section of the horizontal survey. This variation perhaps was due to water moderation having a greater effect than the water absorption over the near center section. This net effect was more pronounced directly over the source.

Figure 14 shows a horizontal x direction comparison at $z = 30$ in. of the wet, dry, and without uranium configurations. Lattice I values of flux for both the wet and dry cases were below the flux values in the no uranium Lattice. The flux in wet Lattice I was again higher than the flux in dry Lattice I. In Lattice I, the absorption effect at the $z = 30$ in. position was obviously greater than the subcritical multiplication effect. Lattice II values of flux for the wet and dry cases are just slightly below the no uranium case. In this lattice the subcritical multiplication effect and the absorption effects were approximately equal.

A lattice comparison for the horizontal x direction at $z = 30$ in. is shown on Figure 15. The Lattice II flux was greater than the Lattice I flux in both the wet and dry configurations.

Symmetry (sine distribution) was shown in the y direction on Figure 16 for Lattices I and II at the $x = 27$ in. and $z = 30$ in. position. The plot shows that there was little difference between the wet and dry cases of either Lattice I

or II. In Lattice I there was an apparent digression from a sine distribution at the center positions of the wet configuration. Also the sine curve plotted for symmetry was slightly to the left of the points plotted on Figure 16. This was probably due to the placement of the foil holders or some spreading of the graphite blocks from a Lattice I loading. The flux plots of the wet and dry configurations in the y direction for Lattice II are approximately the same as the flux plot of the no uranium lattice. There is again some dispersion at the center position in this comparison.

The results of the experimental and theoretical bucklings determined for all configurations considered are shown on Figure 17. The two theoretical methods used to determine the buckling for the dry configurations showed reasonable agreement, but the wet case theory was in disagreement. The results from Method A were high in comparison with the results from Method B for wet Lattices I, II and III.

The experimental buckling values for the wet configurations were lower than the experimental buckling values for the dry configurations in all three lattice spacings investigated. The theoretical values of buckling determined for the dry configurations, Methods A and B, were a little higher than the experimental values of buckling for the dry configurations. The theoretical values of buckling obtained from Method A for the wet configurations were high in comparison with the experimental buckling values. The theoretical Method

B gave buckling values for the wet configurations which were in excellent agreement with the experimental buckling values for the wet lattices.

For the natural uranium graphite assembly a maximum did occur for the wet and dry cases of the buckling versus lattice spacing curve, Figure 17. This maximum occurred in both the experimental and theoretical analyses. The C/U atom ratios were 73 for Lattice I, 146 for Lattice II, and 292 for Lattice III. Davenport (8, p. 315) concluded that the maximum buckling for a given natural uranium fuel assembly should occur at a value of C/U between 50 and 100. The maximum buckling in this investigation of three lattice spacings occurred at about a C/U value of 146 for both the wet and dry configurations.

VI. DISCUSSION OF RESULTS

The theoretical methods employed had the following probable errors. Accurate detailed neutron scattering and capture cross section data are not available in the literature for all materials. Corrections for varying densities and purities of the materials were not computed. A calculated disadvantage factor for uranium was used instead of a measured value. Values from the literature were used for the Fermi age and the various lattice diffusion lengths where experimental values again would have given more accurate results for the calculated buckling. There were cracks between the graphite blocks with a process tube uranium load in the assembly. These air spaces and the air effect around the process tube itself were assumed to be negligible. The effect of temperature and humidity on the results was also assumed to be negligible. Finally, one group neutron theory was used throughout the analysis.

The following comments can be made concerning the experimental methods employed. The harmonic corrections to the flux distributions obtained were assumed to be negligible. The positioning of the foils and the normalizing of the foil activity were subject to human error. Finally, and most important, the slope of the $\ln \phi(z)$ versus z direction curve must be determined with great accuracy. This slope value is very critical in determining the actual buckling. Repeat runs for

consistency at a given position should be taken from which an average value of activities at a position could be used for plotting and the buckling calculation. Varying the foil weight at a given position during the runs would tend to cancel out any normalizing error.

The feasibility of an actual reactor with the process tubing, natural uranium, slug geometry, and water coolant used in this investigation was determined. Assuming 1250 channels, a water coolant, and 0.405 in.^2 flow area per channel the mass flow is $1.68 \times 10^6 \text{ lb/hr.}$ Assuming a temperature difference of 70°F and using $C_p = 1.06$ for water at 400°F , the heat rate transfer is 366 megawatts. This heat rate transfer is large enough for a potential power reactor. The above assumptions are conservative in comparison with the experimental critical reactor volume determined for the wet 8.5 in. lattice configuration.

The process tubing did spread the graphite blocks a small amount due to the fact that some of the holes were smaller than the normal average designed size. A power drill of an appropriate size could enlarge these holes so that the process tubing would slide in and out of the assembly with ease and no spread would occur. It was found that a lattice change was more easily accomplished using the process tube uranium containment than with just the loose slugs. One end of the process tube was beveled to facilitate loading of the wire wrapped slugs. It is suggested that a number seven rubber stopper be

well seated in the beveled end and a larger stopper be used at the other end. Coolant leakage would in this way be eliminated.

The E-3 position foil holder hole was a through hole in the y direction. This through hole would be of more use if it were moved up to the E-8 or E-9 positions. The E-3 position was too close to the source for a good symmetry flux survey.

The 8.5 in. lattice is the optimum lattice spacing which is possible with the subcritical assembly used. Suggested ideas for future study are the investigation of other coolants and a more detailed analysis of the 8.5 in. lattice for both the wet and dry configurations. Also, the effect of the reflection by the water contained below the source may be investigated to give a maximum source flux with the available sources in place. With the use of an additional inner process tube the effect of a variable water annulus could also be investigated.

VII. CONCLUSIONS

The moderation effect of the water was greater than the absorption effect of the water for approximately the lower half of the subcritical assembly for the three lattice spacings investigated. The thermal neutron flux in the lower portion of the assembly was greater in the wet configurations than in the dry configurations, and the reverse situation existed in the upper portion of the assembly. The 6 in. wet lattice had the lowest overall flux because the absorption effect of the greater amount of water and uranium was larger than the subcritical multiplication effect in this lattice. The 12 in. lattice was "over moderated" with an apparent small subcritical multiplication effect. The optimum lattice investigated was the 8.5 in. lattice. In this lattice the water had very little effect on the flux distribution due to the balance of the water moderation and absorption effects.

The symmetry surveys showed that in the x and y directions that the flux did follow a sine distribution for both the wet and dry configurations.

The two theoretical methods used to determine the buckling for the dry configurations gave results with reasonable agreement. These theoretical bucklings for the dry cases were high in comparison with the experimental bucklings determined for the dry cases except for the 12 in. lattice. The two theoretical methods used to determine the buckling for the

[illegible]

wet configurations gave results which were in disagreement. The method of Murray gave values of the buckling for the wet configuration of the 6 in. and 8.5 in. lattices which were very high in comparison with the experimental buckling values. The method of Rumsey and Volkoff gave values of the buckling for the wet configuration of the 6 in. and 8.5 in. lattices which were in excellent agreement with the experimental buckling values determined. The experimental buckling value determined for the 12 in. wet lattice was between the two theoretical buckling values determined for this lattice. The experimental buckling values for the dry cases were higher than the values for the wet cases in all lattice spacings investigated. The only experimental positive value of buckling for the wet configurations was the buckling value for the 8.5 in. lattice.

A maximum in the buckling versus lattice spacing curve did occur for both the wet and dry configurations. This maximum in buckling was found in both the theoretical and the experimental values determined. These buckling curves for the wet and dry configurations did not cross; hence a "fail-safe" behavior upon the loss of water coolant could not be expected from these results.

[illegible]

Table 1

Dimensions for a unit cell

Lattice I (6 in.), II (8.5 in.), and III (12 in.)

r_u ,	uranium rod radius	1.270 cm
t_{al} ,	thickness of aluminum slug can	0.102 cm
t_w ,	effective thickness of water annulus	0.273 cm
t_p ,	effective thickness of process tube	0.102 cm
t_{air} ,	effective thickness of air annulus	0.455 cm
r_1 ,	equivalent inner radius of graphite	2.20 cm

Equivalent cross section areas for one cell

Uranium	5.06 cm ²
Slug can	0.84 cm ²
Water coolant	2.61 cm ²
Process tube	1.06 cm ²
Air	5.65 cm ²
Graphite, Lattice I	217.0 cm ²
Graphite, Lattice II	434.0 cm ²
Graphite, Lattice III	868.0 cm ²

Volume per slug

V_u ,	uranium	103.0 cm ³
V_{al} ,	slug can and cap	23.0 cm ³
V_w ,	water	55.7 cm ³
V_p ,	process tube	22.6 cm ³
V_{g1} ,	graphite, Lattice I	4625 cm ³
V_{g2} ,	graphite, Lattice II	9250 cm ³
V_{g3} ,	graphite, Lattice III	18,500 cm ³

Table 1 (Continued)

Lattice I, r_2 , equivalent outer radius of graphite	8.60 cm
Lattice II, r_2 , equivalent outer radius of graphite	11.94 cm
Lattice III, r_2 , equivalent outer radius of graphite	16.76 cm

Table 2

Lattice cell material constants

Symbol	Value	Source
\sum_a^{al}	0.01323 cm^{-1}	(5) and Equation 25
\sum_a^f	0.01556 cm^{-1}	(5), (11) and Equation 25
\sum_a^u	0.324 cm^{-1}	(1) and Equation 25
\sum_s^u	0.399 cm^{-1}	(1) and Equation 25
\sum_0	0.0967 cm^{-1}	Equation 43
\sum_a^g	0.00036 cm^{-1}	(5)
\sum_s^g	0.375 cm^{-1}	(1) and Equation 25
\sum_1^m	0.01057 cm^{-1}	(1) and Equation 44
\sum_t^g	0.354 cm^{-1}	(1) and Equation 49
\sum_a^w	0.017 cm^{-1}	(5)
H_u	0.675 cm^{-1}	Equation 26
H_g	0.01992 cm^{-1}	(5) and Equation 27

Table 2 (Continued)

Symbol	Value	Source
η_w	0.3472 cm^{-1}	(5) and Equation 27
η_u^{re}	0.4218 cm^{-1}	Equation 46
η_g^{re}	0.1059 cm^{-1}	Equation 47
$\overline{\cos \theta}$	0.0555	Equation 50
q_w/q_g	20	(3)
f_g	0.158	(5)
Fermi age, τ_g	364 cm^2	(1)
L_g^2	2520 cm^2	(1)
ρ_g	1.56 g/cm^3	Measured value
ρ_u	19.0 g/cm^3	Measured value
S/M	$.0828 \text{ cm}^2/\text{gm}$	Calculated value, Equation 42

(continued) Table 1

Location	Depth	Length
70 m (223 ft)	1.5 m (4.9 ft)	8
100 m (328 ft)	1.5 m (4.9 ft)	8
130 m (427 ft)	1.5 m (4.9 ft)	8
160 m (525 ft)	1.5 m (4.9 ft)	8
190 m (623 ft)	1.5 m (4.9 ft)	8
220 m (722 ft)	1.5 m (4.9 ft)	8
250 m (820 ft)	1.5 m (4.9 ft)	8
280 m (919 ft)	1.5 m (4.9 ft)	8
310 m (1017 ft)	1.5 m (4.9 ft)	8
340 m (1115 ft)	1.5 m (4.9 ft)	8
370 m (1214 ft)	1.5 m (4.9 ft)	8
400 m (1312 ft)	1.5 m (4.9 ft)	8
430 m (1411 ft)	1.5 m (4.9 ft)	8
460 m (1510 ft)	1.5 m (4.9 ft)	8
490 m (1609 ft)	1.5 m (4.9 ft)	8
520 m (1708 ft)	1.5 m (4.9 ft)	8
550 m (1807 ft)	1.5 m (4.9 ft)	8
580 m (1906 ft)	1.5 m (4.9 ft)	8
610 m (2005 ft)	1.5 m (4.9 ft)	8
640 m (2104 ft)	1.5 m (4.9 ft)	8
670 m (2203 ft)	1.5 m (4.9 ft)	8
700 m (2302 ft)	1.5 m (4.9 ft)	8
730 m (2401 ft)	1.5 m (4.9 ft)	8
760 m (2500 ft)	1.5 m (4.9 ft)	8
790 m (2599 ft)	1.5 m (4.9 ft)	8
820 m (2698 ft)	1.5 m (4.9 ft)	8
850 m (2797 ft)	1.5 m (4.9 ft)	8
880 m (2896 ft)	1.5 m (4.9 ft)	8
910 m (2995 ft)	1.5 m (4.9 ft)	8
940 m (3094 ft)	1.5 m (4.9 ft)	8
970 m (3193 ft)	1.5 m (4.9 ft)	8
1000 m (3292 ft)	1.5 m (4.9 ft)	8
1030 m (3391 ft)	1.5 m (4.9 ft)	8
1060 m (3490 ft)	1.5 m (4.9 ft)	8
1090 m (3589 ft)	1.5 m (4.9 ft)	8
1120 m (3688 ft)	1.5 m (4.9 ft)	8
1150 m (3787 ft)	1.5 m (4.9 ft)	8
1180 m (3886 ft)	1.5 m (4.9 ft)	8
1210 m (3985 ft)	1.5 m (4.9 ft)	8
1240 m (4084 ft)	1.5 m (4.9 ft)	8
1270 m (4183 ft)	1.5 m (4.9 ft)	8
1300 m (4282 ft)	1.5 m (4.9 ft)	8
1330 m (4381 ft)	1.5 m (4.9 ft)	8
1360 m (4480 ft)	1.5 m (4.9 ft)	8
1390 m (4579 ft)	1.5 m (4.9 ft)	8
1420 m (4678 ft)	1.5 m (4.9 ft)	8
1450 m (4777 ft)	1.5 m (4.9 ft)	8
1480 m (4876 ft)	1.5 m (4.9 ft)	8
1510 m (4975 ft)	1.5 m (4.9 ft)	8
1540 m (5074 ft)	1.5 m (4.9 ft)	8
1570 m (5173 ft)	1.5 m (4.9 ft)	8
1600 m (5272 ft)	1.5 m (4.9 ft)	8
1630 m (5371 ft)	1.5 m (4.9 ft)	8
1660 m (5470 ft)	1.5 m (4.9 ft)	8
1690 m (5569 ft)	1.5 m (4.9 ft)	8
1720 m (5668 ft)	1.5 m (4.9 ft)	8
1750 m (5767 ft)	1.5 m (4.9 ft)	8
1780 m (5866 ft)	1.5 m (4.9 ft)	8
1810 m (5965 ft)	1.5 m (4.9 ft)	8
1840 m (6064 ft)	1.5 m (4.9 ft)	8
1870 m (6163 ft)	1.5 m (4.9 ft)	8
1900 m (6262 ft)	1.5 m (4.9 ft)	8
1930 m (6361 ft)	1.5 m (4.9 ft)	8
1960 m (6460 ft)	1.5 m (4.9 ft)	8
1990 m (6559 ft)	1.5 m (4.9 ft)	8
2020 m (6658 ft)	1.5 m (4.9 ft)	8
2050 m (6757 ft)	1.5 m (4.9 ft)	8
2080 m (6856 ft)	1.5 m (4.9 ft)	8
2110 m (6955 ft)	1.5 m (4.9 ft)	8
2140 m (7054 ft)	1.5 m (4.9 ft)	8
2170 m (7153 ft)	1.5 m (4.9 ft)	8
2200 m (7252 ft)	1.5 m (4.9 ft)	8
2230 m (7351 ft)	1.5 m (4.9 ft)	8
2260 m (7450 ft)	1.5 m (4.9 ft)	8
2290 m (7549 ft)	1.5 m (4.9 ft)	8
2320 m (7648 ft)	1.5 m (4.9 ft)	8
2350 m (7747 ft)	1.5 m (4.9 ft)	8
2380 m (7846 ft)	1.5 m (4.9 ft)	8
2410 m (7945 ft)	1.5 m (4.9 ft)	8
2440 m (8044 ft)	1.5 m (4.9 ft)	8
2470 m (8143 ft)	1.5 m (4.9 ft)	8
2500 m (8242 ft)	1.5 m (4.9 ft)	8
2530 m (8341 ft)	1.5 m (4.9 ft)	8
2560 m (8440 ft)	1.5 m (4.9 ft)	8
2590 m (8539 ft)	1.5 m (4.9 ft)	8
2620 m (8638 ft)	1.5 m (4.9 ft)	8
2650 m (8737 ft)	1.5 m (4.9 ft)	8
2680 m (8836 ft)	1.5 m (4.9 ft)	8
2710 m (8935 ft)	1.5 m (4.9 ft)	8
2740 m (9034 ft)	1.5 m (4.9 ft)	8
2770 m (9133 ft)	1.5 m (4.9 ft)	8
2800 m (9232 ft)	1.5 m (4.9 ft)	8
2830 m (9331 ft)	1.5 m (4.9 ft)	8
2860 m (9430 ft)	1.5 m (4.9 ft)	8
2890 m (9529 ft)	1.5 m (4.9 ft)	8
2920 m (9628 ft)	1.5 m (4.9 ft)	8
2950 m (9727 ft)	1.5 m (4.9 ft)	8
2980 m (9826 ft)	1.5 m (4.9 ft)	8
3010 m (9925 ft)	1.5 m (4.9 ft)	8
3040 m (10024 ft)	1.5 m (4.9 ft)	8
3070 m (10123 ft)	1.5 m (4.9 ft)	8
3100 m (10222 ft)	1.5 m (4.9 ft)	8
3130 m (10321 ft)	1.5 m (4.9 ft)	8
3160 m (10420 ft)	1.5 m (4.9 ft)	8
3190 m (10519 ft)	1.5 m (4.9 ft)	8
3220 m (10618 ft)	1.5 m (4.9 ft)	8
3250 m (10717 ft)	1.5 m (4.9 ft)	8
3280 m (10816 ft)	1.5 m (4.9 ft)	8
3310 m (10915 ft)	1.5 m (4.9 ft)	8
3340 m (11014 ft)	1.5 m (4.9 ft)	8
3370 m (11113 ft)	1.5 m (4.9 ft)	8
3400 m (11212 ft)	1.5 m (4.9 ft)	8
3430 m (11311 ft)	1.5 m (4.9 ft)	8
3460 m (11410 ft)	1.5 m (4.9 ft)	8
3490 m (11509 ft)	1.5 m (4.9 ft)	8
3520 m (11608 ft)	1.5 m (4.9 ft)	8
3550 m (11707 ft)	1.5 m (4.9 ft)	8
3580 m (11806 ft)	1.5 m (4.9 ft)	8
3610 m (11905 ft)	1.5 m (4.9 ft)	8
3640 m (12004 ft)	1.5 m (4.9 ft)	8
3670 m (12103 ft)	1.5 m (4.9 ft)	8
3700 m (12202 ft)	1.5 m (4.9 ft)	8
3730 m (12301 ft)	1.5 m (4.9 ft)	8
3760 m (12400 ft)	1.5 m (4.9 ft)	8
3790 m (12499 ft)	1.5 m (4.9 ft)	8
3820 m (12598 ft)	1.5 m (4.9 ft)	8
3850 m (12697 ft)	1.5 m (4.9 ft)	8
3880 m (12796 ft)	1.5 m (4.9 ft)	8
3910 m (12895 ft)	1.5 m (4.9 ft)	8
3940 m (12994 ft)	1.5 m (4.9 ft)	8
3970 m (13093 ft)	1.5 m (4.9 ft)	8
4000 m (13192 ft)	1.5 m (4.9 ft)	8
4030 m (13291 ft)	1.5 m (4.9 ft)	8
4060 m (13390 ft)	1.5 m (4.9 ft)	8
4090 m (13489 ft)	1.5 m (4.9 ft)	8
4120 m (13588 ft)	1.5 m (4.9 ft)	8
4150 m (13687 ft)	1.5 m (4.9 ft)	8
4180 m (13786 ft)	1.5 m (4.9 ft)	8
4210 m (13885 ft)	1.5 m (4.9 ft)	8
4240 m (13984 ft)	1.5 m (4.9 ft)	8
4270 m (14083 ft)	1.5 m (4.9 ft)	8
4300 m (14182 ft)	1.5 m (4.9 ft)	8
4330 m (14281 ft)	1.5 m (4.9 ft)	8
4360 m (14380 ft)	1.5 m (4.9 ft)	8
4390 m (14479 ft)	1.5 m (4.9 ft)	8
4420 m (14578 ft)	1.5 m (4.9 ft)	8
4450 m (14677 ft)	1.5 m (4.9 ft)	8
4480 m (14776 ft)	1.5 m (4.9 ft)	8
4510 m (14875 ft)	1.5 m (4.9 ft)	8
4540 m (14974 ft)	1.5 m (4.9 ft)	8
4570 m (15073 ft)	1.5 m (4.9 ft)	8
4600 m (15172 ft)	1.5 m (4.9 ft)	8
4630 m (15271 ft)	1.5 m (4.9 ft)	8
4660 m (15370 ft)	1.5 m (4.9 ft)	8
4690 m (15469 ft)	1.5 m (4.9 ft)	8
4720 m (15568 ft)	1.5 m (4.9 ft)	8
4750 m (15667 ft)	1.5 m (4.9 ft)	8
4780 m (15766 ft)	1.5 m (4.9 ft)	8
4810 m (15865 ft)	1.5 m (4.9 ft)	8
4840 m (15964 ft)	1.5 m (4.9 ft)	8
4870 m (16063 ft)	1.5 m (4.9 ft)	8
4900 m (16162 ft)	1.5 m (4.9 ft)	8
4930 m (16261 ft)	1.5 m (4.9 ft)	8
4960 m (16360 ft)	1.5 m (4.9 ft)	8
4990 m (16459 ft)	1.5 m (4.9 ft)	8
5020 m (16558 ft)	1.5 m (4.9 ft)	8
5050 m (16657 ft)	1.5 m (4.9 ft)	8
5080 m (16756 ft)	1.5 m (4.9 ft)	8
5110 m (16855 ft)	1.5 m (4.9 ft)	8
5140 m (16954 ft)	1.5 m (4.9 ft)	8
5170 m (17053 ft)	1.5 m (4.9 ft)	8
5200 m (17152 ft)	1.5 m (4.9 ft)	8
5230 m (17251 ft)	1.5 m (4.9 ft)	8
5260 m (17350 ft)	1.5 m (4.9 ft)	8
5290 m (17449 ft)	1.5 m (4.9 ft)	8
5320 m (17548 ft)	1.5 m (4.9 ft)	8
5350 m (17647 ft)	1.5 m (4.9 ft)	8
5380 m (17746 ft)	1.5 m (4.9 ft)	8
5410 m (17845 ft)	1.5 m (4.9 ft)	8
5440 m (17944 ft)	1.5 m (4.9 ft)	8
5470 m (18043 ft)	1.5 m (4.9 ft)	8
5500 m (18142 ft)	1.5 m (4.9 ft)	8
5530 m (18241 ft)	1.5 m (4.9 ft)	8
5560 m (18340 ft)	1.5 m (4.9 ft)	8
5590 m (18439 ft)	1.5 m (4.9 ft)	8
5620 m (18538 ft)	1.5 m (4.9 ft)	8
5650 m (18637 ft)	1.5 m (4.9 ft)	8
5680 m (18736 ft)	1.5 m (4.9 ft)	8
5710 m (18835 ft)	1.5 m (4.9 ft)	8
5740 m (18934 ft)	1.5 m (4.9 ft)	8
5770 m (19033 ft)	1.5 m (4.9 ft)	8
5800 m (19132 ft)	1.5 m (4.9 ft)	8
5830 m (19231 ft)	1.5 m (4.9 ft)	8
5860 m (19330 ft)	1.5 m (4.9 ft)	8
5890 m (19429 ft)	1.5 m (4.9 ft)	8
5920 m (19528 ft)	1.5 m (4.9 ft)	8
5950 m (19627 ft)	1.5 m (4.9 ft)	8
5980 m (19726 ft)	1.5 m (4.9 ft)	8
6010 m (19825 ft)	1.5 m (4.9 ft)	8
6040 m (19924 ft)	1.5 m (4.9 ft)	8
6070 m (20023 ft)	1.5 m (4.9 ft)	8
6100 m (20122 ft)	1.5 m (4.9 ft)	8
6130 m (20221 ft)	1.5 m (4.9 ft)	8
6160 m (20320 ft)	1.5 m (4.9 ft)	8
6190 m (20419 ft)	1.5 m (4.9 ft)	8
6220 m (20518 ft)	1.5 m (4.9 ft)	8
6250 m (20617 ft)	1.5 m (4.9 ft)	8
6280 m (20716 ft)	1.5 m (4.9 ft)	8
6310 m (20815 ft)	1.5 m (4.9 ft)	8
6340 m (20914 ft)	1.5 m (4.9 ft)	8
6370 m (21013 ft)	1.5 m (4.9 ft)	8
6400 m (21112 ft)	1.5 m (4.9 ft)	8
6430 m (21211 ft)	1.5 m (4.9 ft)	8
6460 m (21310 ft)	1.5 m (4.9 ft)	8
6490 m (21409 ft)	1.5 m (4.9 ft)	8
6520 m (21508 ft)	1.5 m (4.9 ft)	8
6550 m (21607 ft)	1.5 m (4.9 ft)	8
6580 m (21706 ft)	1.5 m (4.9 ft)	8
6610 m (21805 ft)	1.5 m (4.9 ft)	8
6640 m (21904 ft)	1.5 m (4.9 ft)	8
6670 m (22003 ft)	1.5 m (4.9 ft)	8
6700 m (22102 ft)	1.5 m (4.9 ft)	8
6730 m (22201 ft)	1.5 m (4.9 ft)	8
6760 m (22300 ft)	1.5 m (4.9 ft)	8
6790 m (22399 ft)	1.5 m (4.9 ft)	8
6820 m (22498 ft)	1.5 m (4.9 ft)	8
6850 m (22597 ft)	1.5 m (4.9 ft)	8
6880 m (22696 ft)	1.5 m (4.9 ft)	8
6910 m (22795 ft)	1.5 m (4.9 ft)	8
6940 m (22894 ft)	1.5 m (4.9 ft)	8
6970 m (22993 ft)	1.5 m (4.9 ft)	8
7000 m (23092 ft)	1.5 m (4.9 ft)	8
7030 m (23191 ft)	1.5 m (4.9 ft)	8
7060 m (23290 ft)	1.5 m (4.9 ft)	8
7090 m (23389 ft)	1.5 m (4.9 ft)	8
7120 m (23488 ft)	1.5 m (4.9 ft)	8
7150 m (23587 ft)	1.5 m (4.9 ft)	8
7180 m (23686 ft)	1.5 m (4.9 ft)	8
7210 m (23785 ft)	1.5 m (4.9 ft)	8
7240 m (23884 ft)	1.5 m (4.9 ft)	8
7270 m (23983 ft)	1.5 m (4.9 ft)	8
7300 m (24082 ft)	1.5 m (4.9 ft)	8
7330 m (24181 ft)	1.5 m (4.9 ft)	8
7360 m (24280 ft)	1.5 m (4.9 ft)	8
7390 m (24379 ft)	1.5 m (4.9 ft)	8
7420 m (24478 ft)	1.5 m (4.9 ft)	8
7450 m (24577 ft)	1.5 m (4.9 ft)	8
7480 m (24676 ft)	1.5 m (4.9 ft)	8
7510 m (24775 ft)	1.5 m (4.9 ft)	8
7540 m (24874 ft)	1.5 m (4.9 ft)	8
7570 m (24973 ft)	1.5 m (4.9 ft)	8
7600 m (25072 ft)	1.5 m (4.9 ft)	8
7630 m (25171 ft)	1.5 m (4.9 ft)	8
7660 m (25270 ft)	1.5 m (4.9 ft)	8
7690 m (25369 ft)	1.5 m (4.9 ft)	8
7720 m (25468 ft)	1.5 m (4.9 ft)	8
7750 m (25567 ft)	1.5 m (4.9 ft)	8
7780 m (25666 ft)	1.5 m (4.9 ft)	8
7810 m (25765 ft)	1.5 m (4.9 ft)	8
7840 m (25864 ft)	1.5 m (4.9 ft)	8
7870 m (25963 ft)	1.5 m (4.9 ft)	8
7900 m (26062 ft)	1.5 m (4.9 ft)	8
7930 m (26161 ft)	1.5 m (4.9 ft)	8
7960 m (26260 ft)	1.5 m (4.9 ft)	8
7990 m (26359 ft)	1.5 m (4.9 ft)	8
8020 m (26458 ft)	1.5 m (4.9 ft)	8
8050 m (26557 ft)	1.5 m (4.9 ft)	8
8080 m (26656 ft)	1.5 m (4.9 ft)	8
8110 m (26755 ft)	1.5 m (4.9 ft)	8
8140 m (26854 ft)	1.5 m (4.9 ft)	8
8170 m (26953 ft)	1.5 m (4.9 ft)	8
8200 m (27052 ft)	1.5 m (4.9 ft)	8
8230 m (27151 ft)	1.5 m (4.9 ft)	8
8260 m (27250 ft)	1.5 m (4.9 ft)	8
8290 m (27349 ft)	1.5 m (4.9 ft)	8
8320 m (27448 ft)	1.5 m (4.9 ft)	8
8350 m (27547 ft)	1.5 m (4.9 ft)	8
8380 m (27646 ft)	1.5 m (4.9 ft)	8
8410 m (27745 ft)	1.5 m (4.9 ft)	8
8440 m (27844 ft)	1.5 m (4.9 ft)	8
8470 m (27943 ft)	1.5 m (4.9 ft)	8
8500 m (28042 ft)	1.5 m (4.9 ft)	8
8530 m (28141 ft)	1.5 m (4.9 ft)	8
8560 m (28240 ft)	1.5 m (4.9 ft)	8
8590 m (28339 ft)	1.5 m (4.9 ft)	8
8620 m (28438 ft)	1.5 m (4.9 ft)	8
8650 m (28537 ft)	1.5 m (4.9 ft)	8
8680 m (28636 ft)	1.5 m (4.9 ft)	8
8710 m (28735 ft)		

Table 3
Theoretical nuclear lattice constants

Lattice	<u>Method A</u>		
	I	II	III
<u>DRY</u>			
f	0.926	0.870	0.767
p	0.823	0.909	0.955
k_{∞}^*	1.023	1.062	0.984
<u>WET</u>			
f	0.901	0.847	0.751
p	0.823	0.909	0.955
k_{∞}^*	0.996	1.035	0.963
.....			
Lattice	<u>Method B</u>		
	I	II	III
<u>DRY</u>			
f	0.920	0.863	0.759
p	0.836	0.915	0.958
k_{∞}^*	1.034	1.061	0.976
<u>WET</u>			
f	0.882	0.818	0.710
p	0.832	0.911	0.954
k_{∞}^*	0.985	1.008	0.910

*Evaluated using $\epsilon = 1.027$ and $\eta = 1.308$.

TABLE I. *Continuum limit of the lattice action*

Lattice action			
S_L	S_F	S_B	Continuum
S_L			
$S_L^{(1)}$	$S_L^{(2)}$	$S_L^{(3)}$	1
$S_L^{(4)}$	$S_L^{(5)}$	$S_L^{(6)}$	2
$S_L^{(7)}$	$S_L^{(8)}$	$S_L^{(9)}$	3
S_F			
$S_F^{(1)}$	$S_F^{(2)}$	$S_F^{(3)}$	4
$S_F^{(4)}$	$S_F^{(5)}$	$S_F^{(6)}$	5
$S_F^{(7)}$	$S_F^{(8)}$	$S_F^{(9)}$	6
S_B			
$S_B^{(1)}$	$S_B^{(2)}$	$S_B^{(3)}$	7
$S_B^{(4)}$	$S_B^{(5)}$	$S_B^{(6)}$	8
$S_B^{(7)}$	$S_B^{(8)}$	$S_B^{(9)}$	9

Continuum limit of the lattice action

Table 4

Buckling and critical reactor size

Lattice	<u>Theoretical Method A</u>		
	I	II	III
DRY Value			
$L^2 \text{ cm}^2$	186	328	587
$B_m^2 \text{ cm}^{-2}$	41×10^{-6}	86×10^{-6}	-17×10^{-6}
$V_T \text{ cm}^3$	611×10^6	200×10^6	-
Cube side, ft.	27.7	19.2	-
WET Value			
$L^2 \text{ cm}^2$	250	386	627
$B_m^2 \text{ cm}^{-2}$	-6.5×10^{-6}	46×10^{-6}	-37×10^{-6}
$V_T \text{ cm}^3$	-	520×10^6	-
Cube side, ft.	-	26.4	-
Lattice	<u>Theoretical Method B</u>		
	I	II	III
DRY Value			
$L^2 \text{ cm}^2$	201	345	607
$B_m^2 \text{ cm}^{-2}$	59×10^{-6}	83×10^{-6}	-25×10^{-6}
$V_T \text{ cm}^3$	357×10^6	212×10^6	-
Cube side, ft.	23.2	19.6	-
WET Value			
$L^2 \text{ cm}^2$	298	459	730
$B_m^2 \text{ cm}^{-2}$	-23×10^{-6}	9.7×10^{-6}	-85×10^{-6}
$V_T \text{ cm}^3$	-	5340×10^6	-
Cube side, ft.	-	57.4	-

Table 4 (Continued)

Lattice	<u>Experimental</u>		
	I	II	III
DRY Value			
$B_m^2 \text{ cm}^{-2}$	35×10^{-6}	70×10^{-6}	-5×10^{-6}
$V_T \text{ cm}^3$	778×10^6	275×10^6	-
Cube side, ft.	30.1	21.3	-
WET Value			
$B_m^2 \text{ cm}^{-2}$	-23×10^{-6}	12×10^{-6}	-48×10^{-6}
$V_T \text{ cm}^3$	-	3880×10^6	-
Cube side, ft.	-	51.5	-

LIBRARY OF THE

UNIVERSITY OF CHICAGO

181	182	183	184
$\log_{10} 2 = .30103$	$\log_{10} 3 = .47712$	$\log_{10} 4 = .60206$	$\log_{10} 5 = .69897$
$\log_{10} 6 = .77815$	$\log_{10} 7 = .84510$	$\log_{10} 8 = .90309$	$\log_{10} 9 = .95424$
$\log_{10} 10 = 1.00000$	$\log_{10} 11 = 1.04139$	$\log_{10} 12 = 1.07918$	$\log_{10} 13 = 1.11394$
$\log_{10} 14 = 1.14613$	$\log_{10} 15 = 1.17609$	$\log_{10} 16 = 1.20412$	$\log_{10} 17 = 1.23045$
$\log_{10} 18 = 1.25527$	$\log_{10} 19 = 1.27919$	$\log_{10} 20 = 1.30103$	$\log_{10} 21 = 1.32222$
$\log_{10} 22 = 1.34244$	$\log_{10} 23 = 1.36173$	$\log_{10} 24 = 1.38021$	$\log_{10} 25 = 1.39794$
$\log_{10} 26 = 1.41492$	$\log_{10} 27 = 1.43136$	$\log_{10} 28 = 1.44715$	$\log_{10} 29 = 1.46239$
$\log_{10} 30 = 1.47712$	$\log_{10} 31 = 1.49136$	$\log_{10} 32 = 1.50515$	$\log_{10} 33 = 1.51851$
$\log_{10} 34 = 1.53147$	$\log_{10} 35 = 1.54407$	$\log_{10} 36 = 1.55630$	$\log_{10} 37 = 1.56820$
$\log_{10} 38 = 1.57993$	$\log_{10} 39 = 1.59106$	$\log_{10} 40 = 1.60206$	$\log_{10} 41 = 1.61278$
$\log_{10} 42 = 1.62325$	$\log_{10} 43 = 1.63347$	$\log_{10} 44 = 1.64345$	$\log_{10} 45 = 1.65321$
$\log_{10} 46 = 1.66276$	$\log_{10} 47 = 1.67209$	$\log_{10} 48 = 1.68119$	$\log_{10} 49 = 1.69005$
$\log_{10} 50 = 1.69897$	$\log_{10} 51 = 1.70757$	$\log_{10} 52 = 1.71694$	$\log_{10} 53 = 1.72607$
$\log_{10} 54 = 1.73497$	$\log_{10} 55 = 1.74364$	$\log_{10} 56 = 1.75209$	$\log_{10} 57 = 1.76031$
$\log_{10} 58 = 1.76831$	$\log_{10} 59 = 1.77619$	$\log_{10} 60 = 1.78384$	$\log_{10} 61 = 1.79129$
$\log_{10} 62 = 1.79854$	$\log_{10} 63 = 1.80565$	$\log_{10} 64 = 1.81254$	$\log_{10} 65 = 1.81921$
$\log_{10} 66 = 1.82565$	$\log_{10} 67 = 1.83186$	$\log_{10} 68 = 1.83784$	$\log_{10} 69 = 1.84360$
$\log_{10} 70 = 1.84919$	$\log_{10} 71 = 1.85454$	$\log_{10} 72 = 1.85964$	$\log_{10} 73 = 1.86451$
$\log_{10} 74 = 1.86915$	$\log_{10} 75 = 1.87354$	$\log_{10} 76 = 1.87769$	$\log_{10} 77 = 1.88159$
$\log_{10} 78 = 1.88525$	$\log_{10} 79 = 1.88888$	$\log_{10} 80 = 1.89224$	$\log_{10} 81 = 1.89539$
$\log_{10} 82 = 1.89832$	$\log_{10} 83 = 1.90116$	$\log_{10} 84 = 1.90380$	$\log_{10} 85 = 1.90624$
$\log_{10} 86 = 1.90848$	$\log_{10} 87 = 1.91054$	$\log_{10} 88 = 1.91241$	$\log_{10} 89 = 1.91409$
$\log_{10} 90 = 1.91556$	$\log_{10} 91 = 1.91694$	$\log_{10} 92 = 1.91813$	$\log_{10} 93 = 1.91914$
$\log_{10} 94 = 1.92007$	$\log_{10} 95 = 1.92092$	$\log_{10} 96 = 1.92168$	$\log_{10} 97 = 1.92236$
$\log_{10} 98 = 1.92296$	$\log_{10} 99 = 1.92347$	$\log_{10} 100 = 1.92388$	

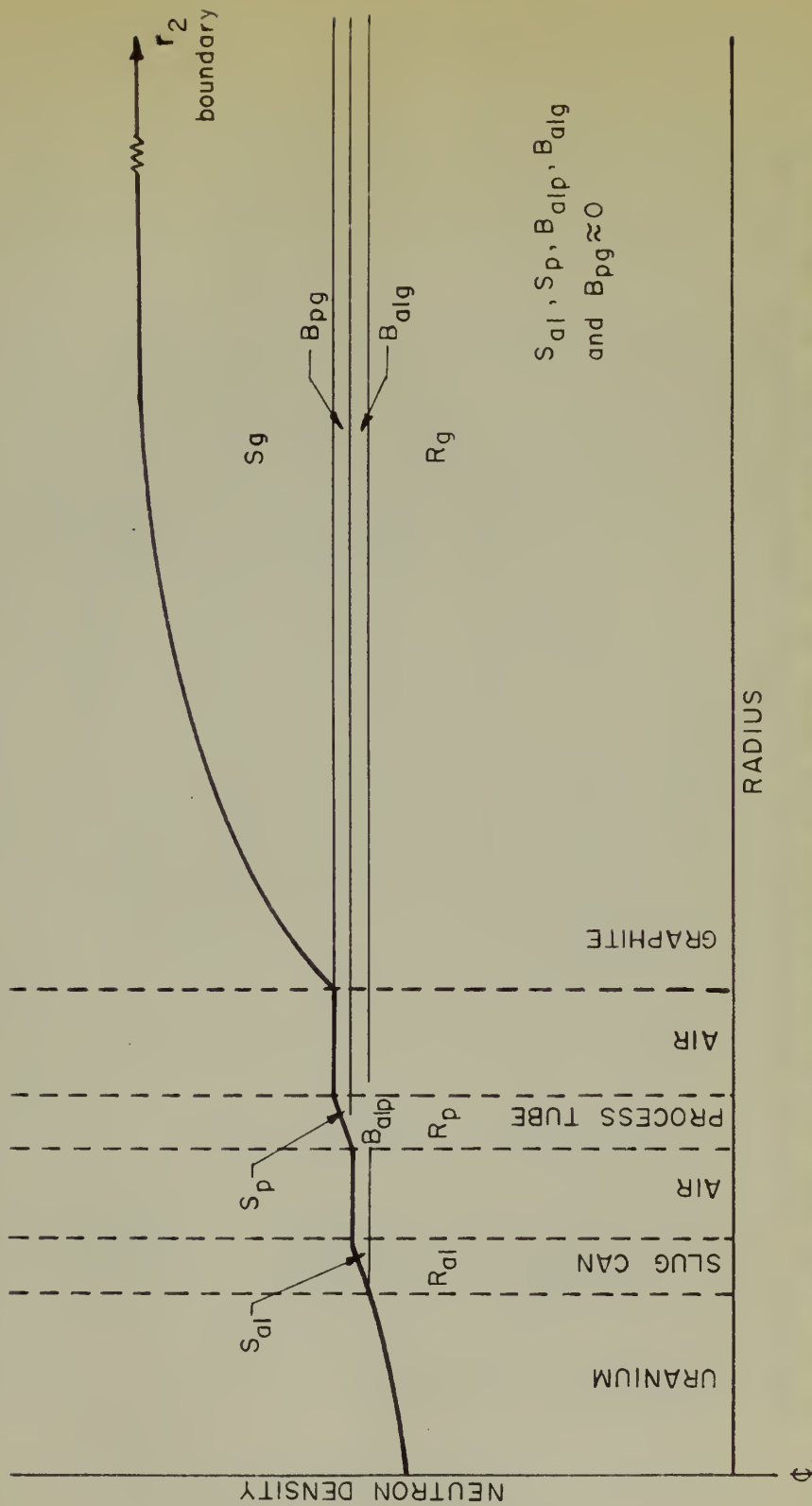


Figure 1. Neutron distribution in a uranium graphite aluminum lattice, dry configuration.

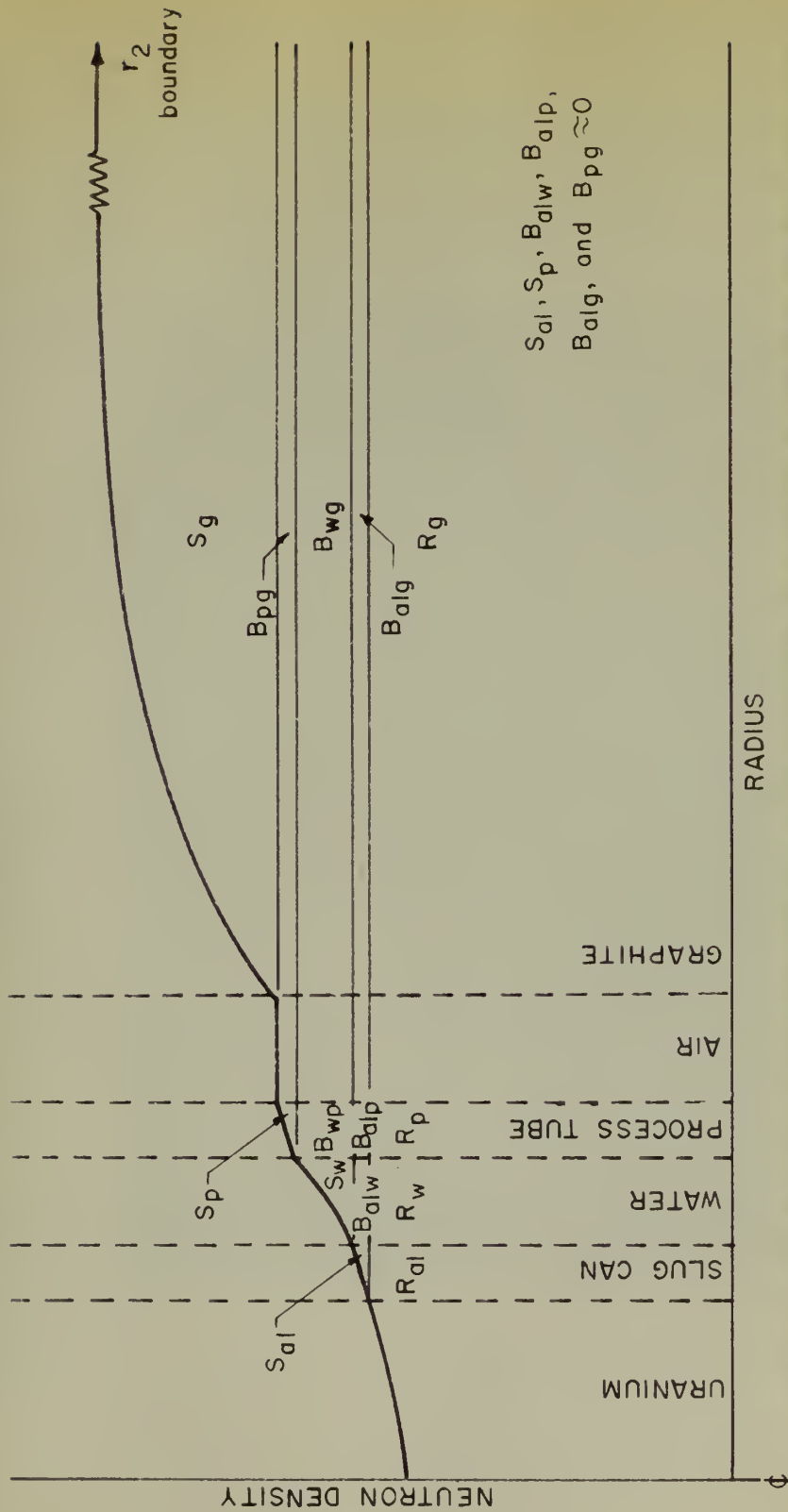
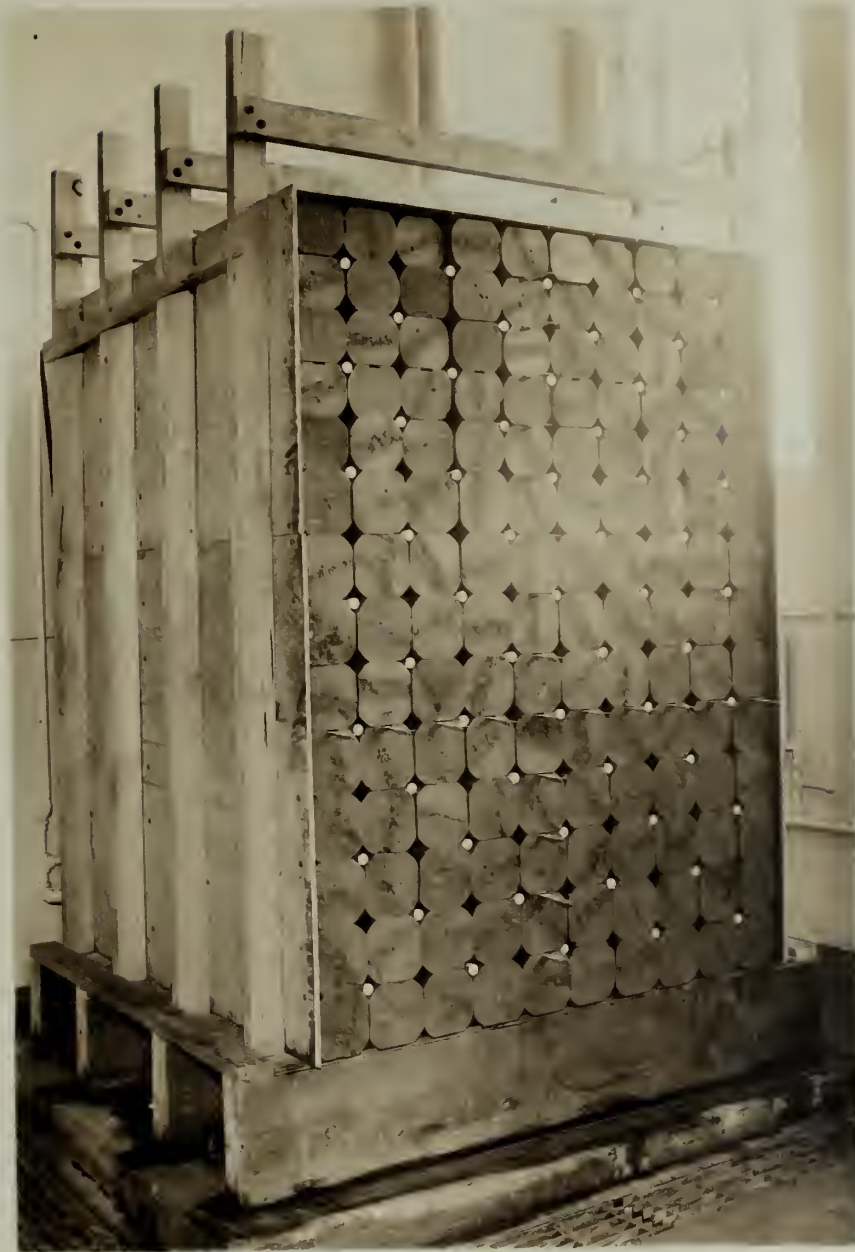


Figure 2. Neutron distribution in a uranium graphite aluminum water lattice, wet configuration.

Adiantum punctatum L. var. *viridifolium*

Figure 3. Subcritical assembly



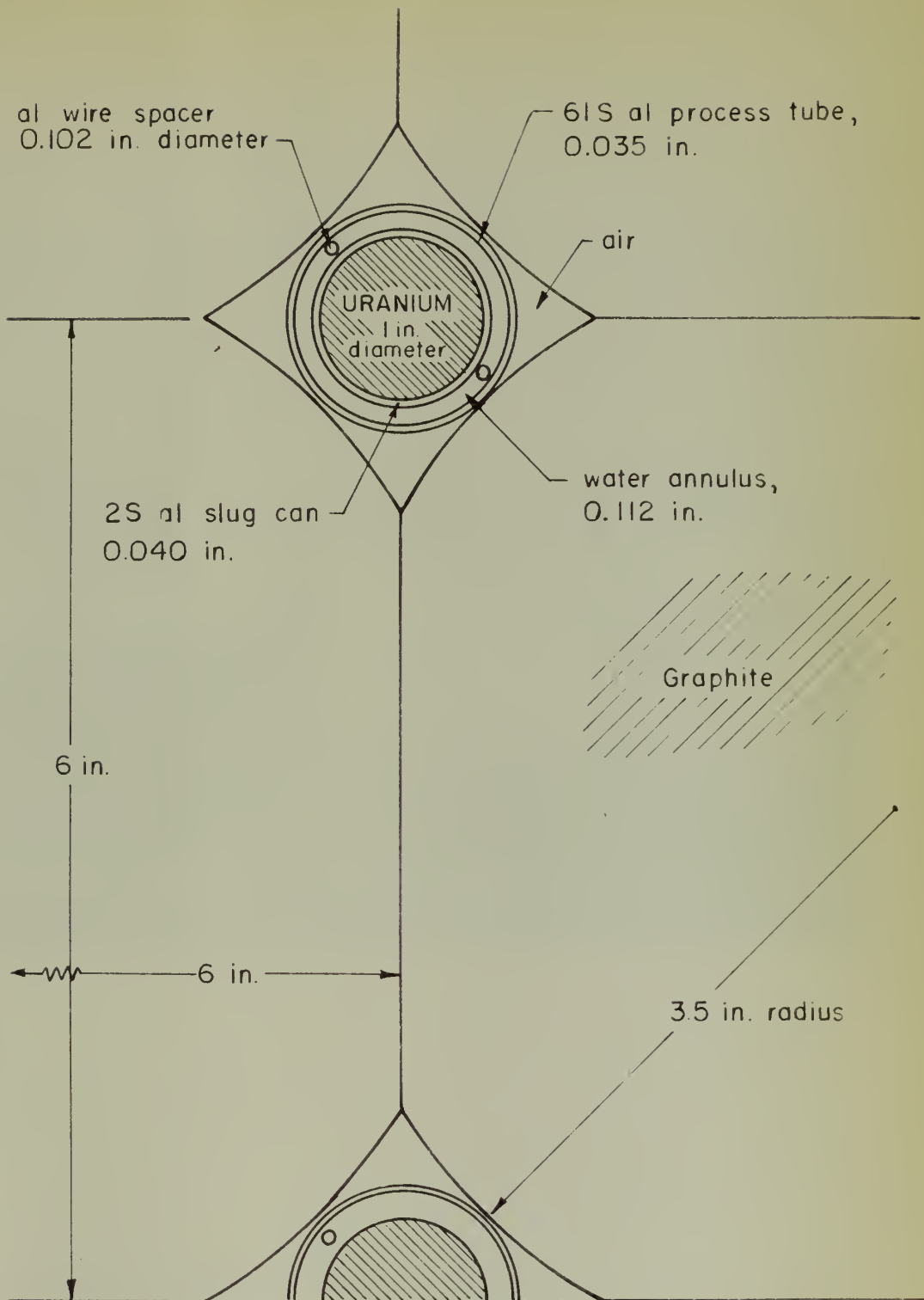
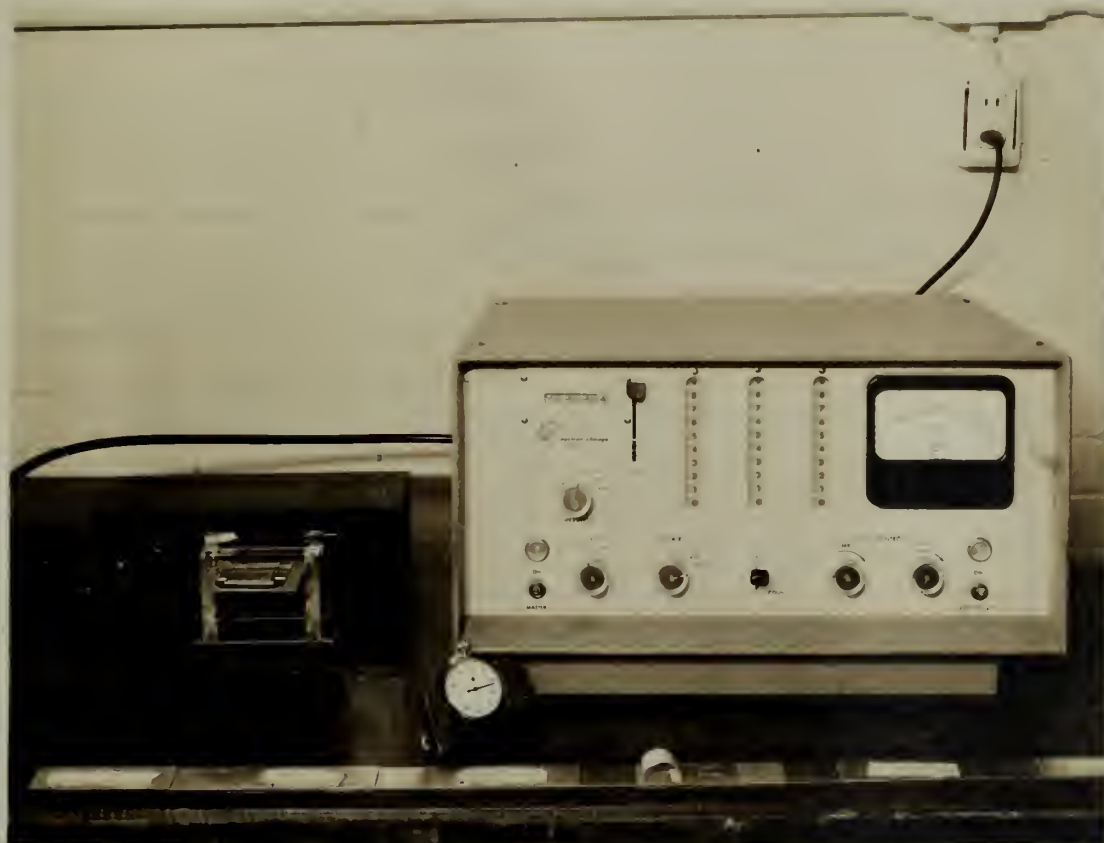


Figure 4. Actual unit cell.

— 1881 —

Figure 5. Counting equipment.



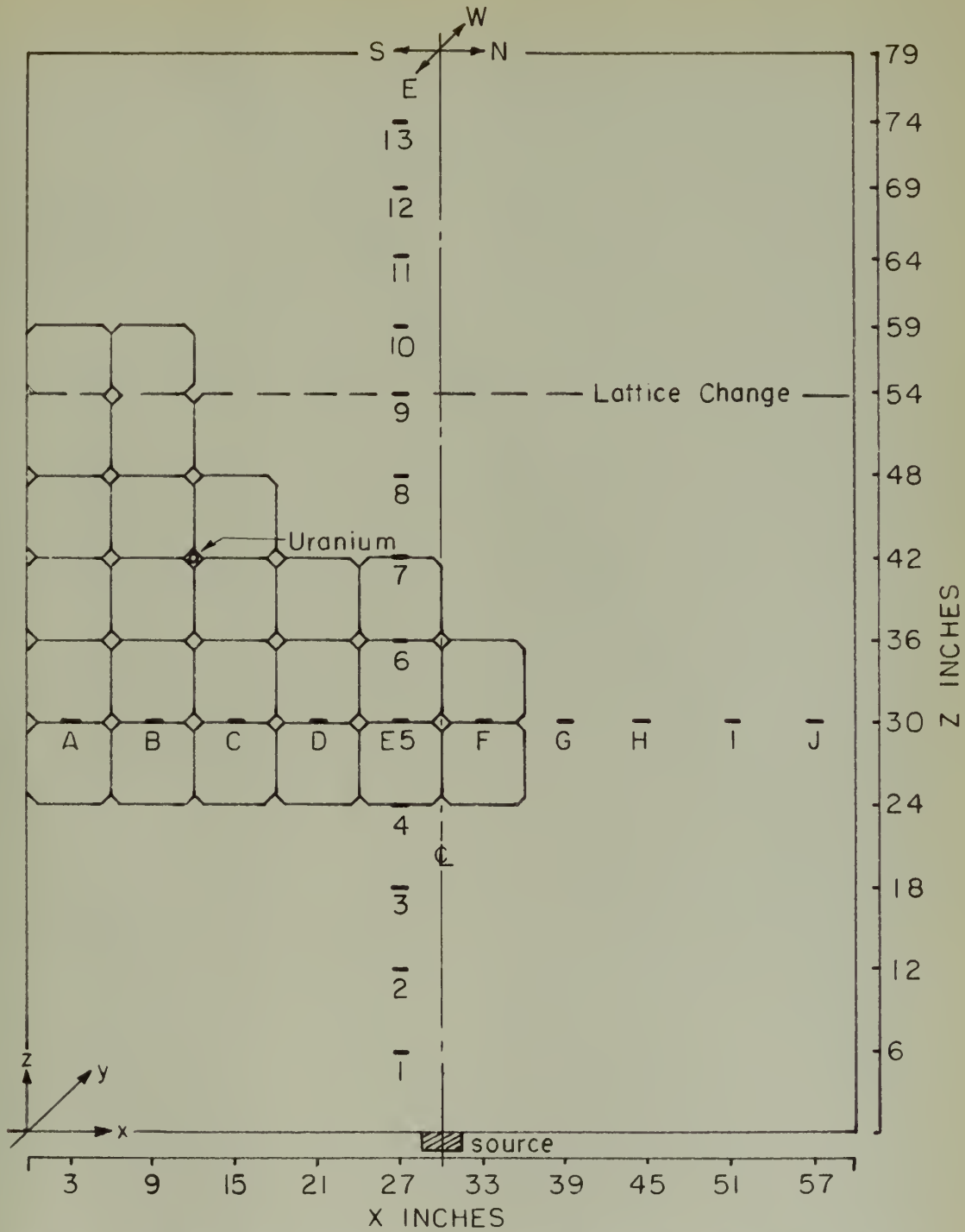


Figure 6. Front view of assembly showing foil positions.

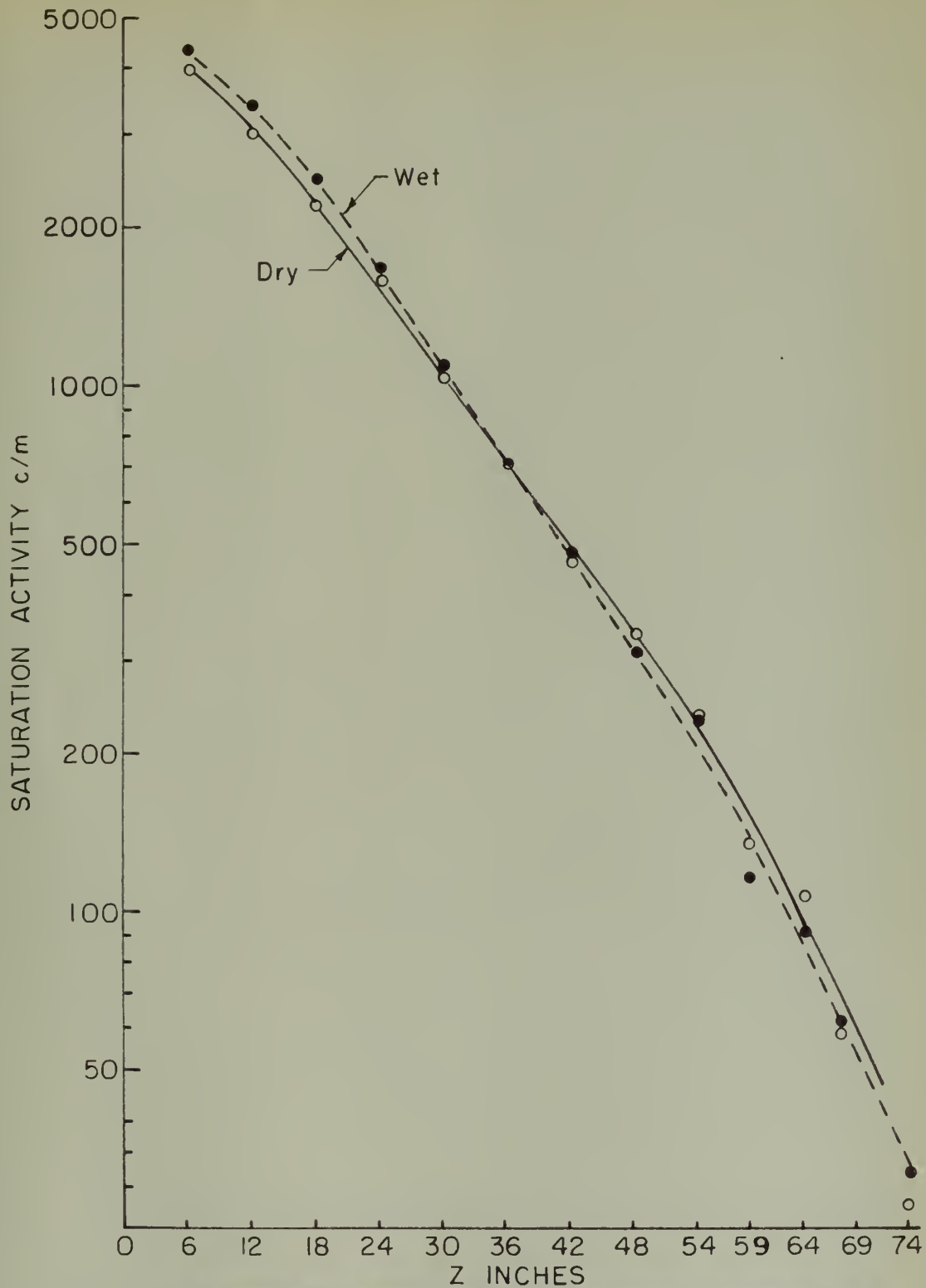


Figure 7. Vertical flux survey, Lattice I,
 $x = 27$ in., $y = 18$ in.

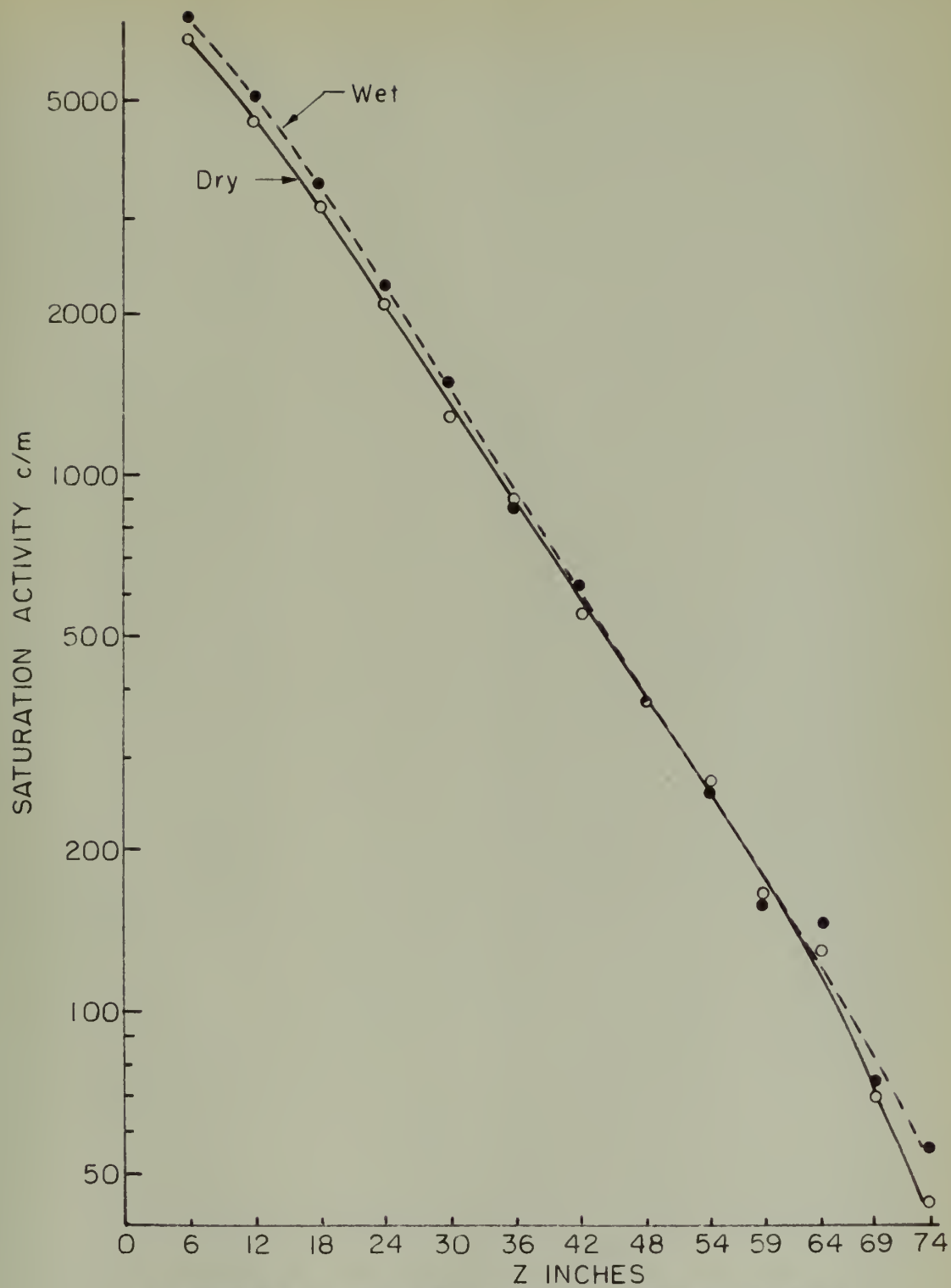


Figure 8. Vertical flux survey, Lattice I,
 $x = 27$ in., $y = 30$ in.

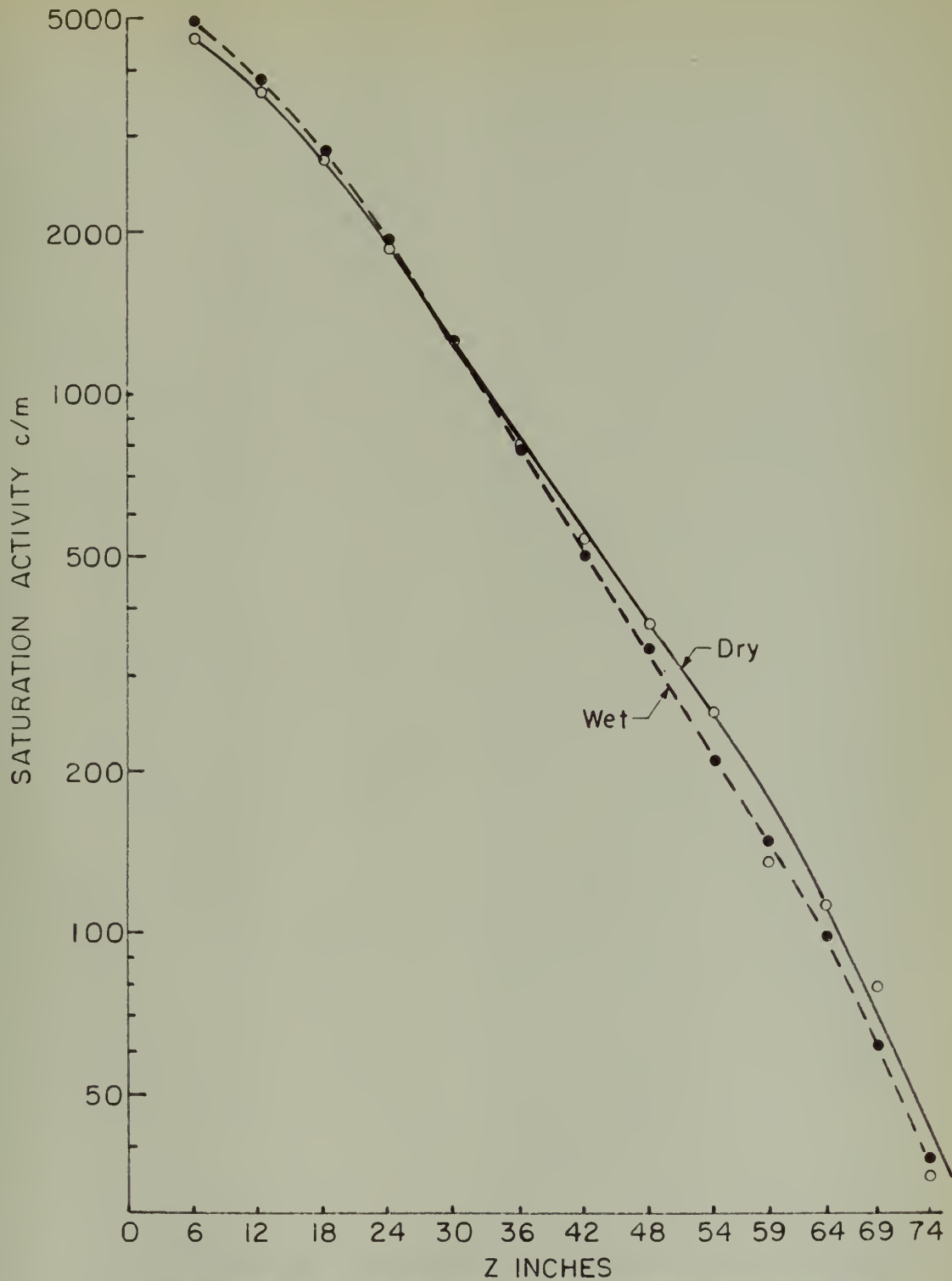


Figure 9. Vertical flux survey, Lattice II,
 $x = 27$ in., $y = 18$ in.

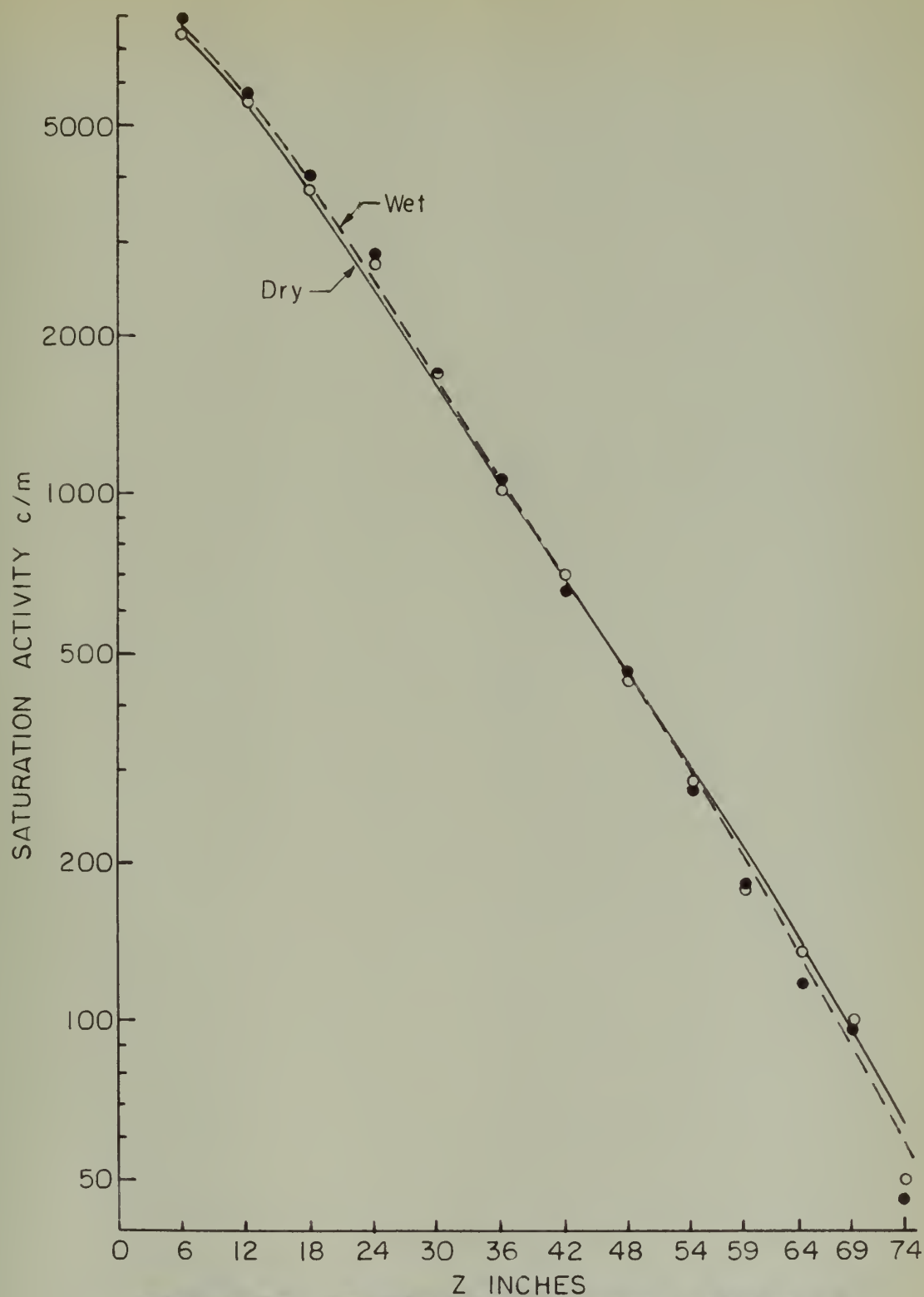


Figure 10. Vertical flux survey, Lattice II,
 $x = 27$ in., $y = 30$ in.

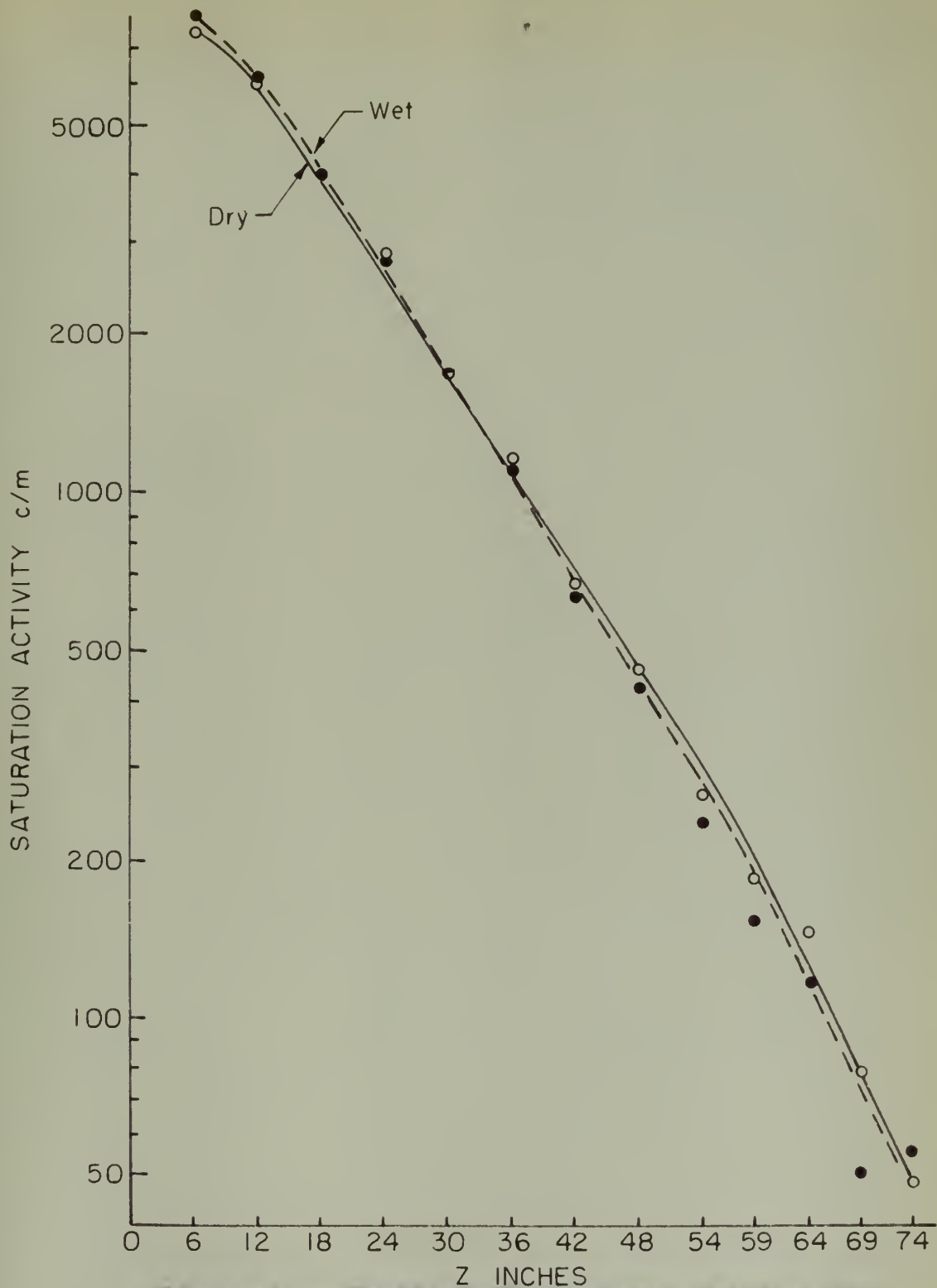


Figure 11. Vertical flux survey, Lattice III,
 $x = 27$ in., $y = 30$ in.

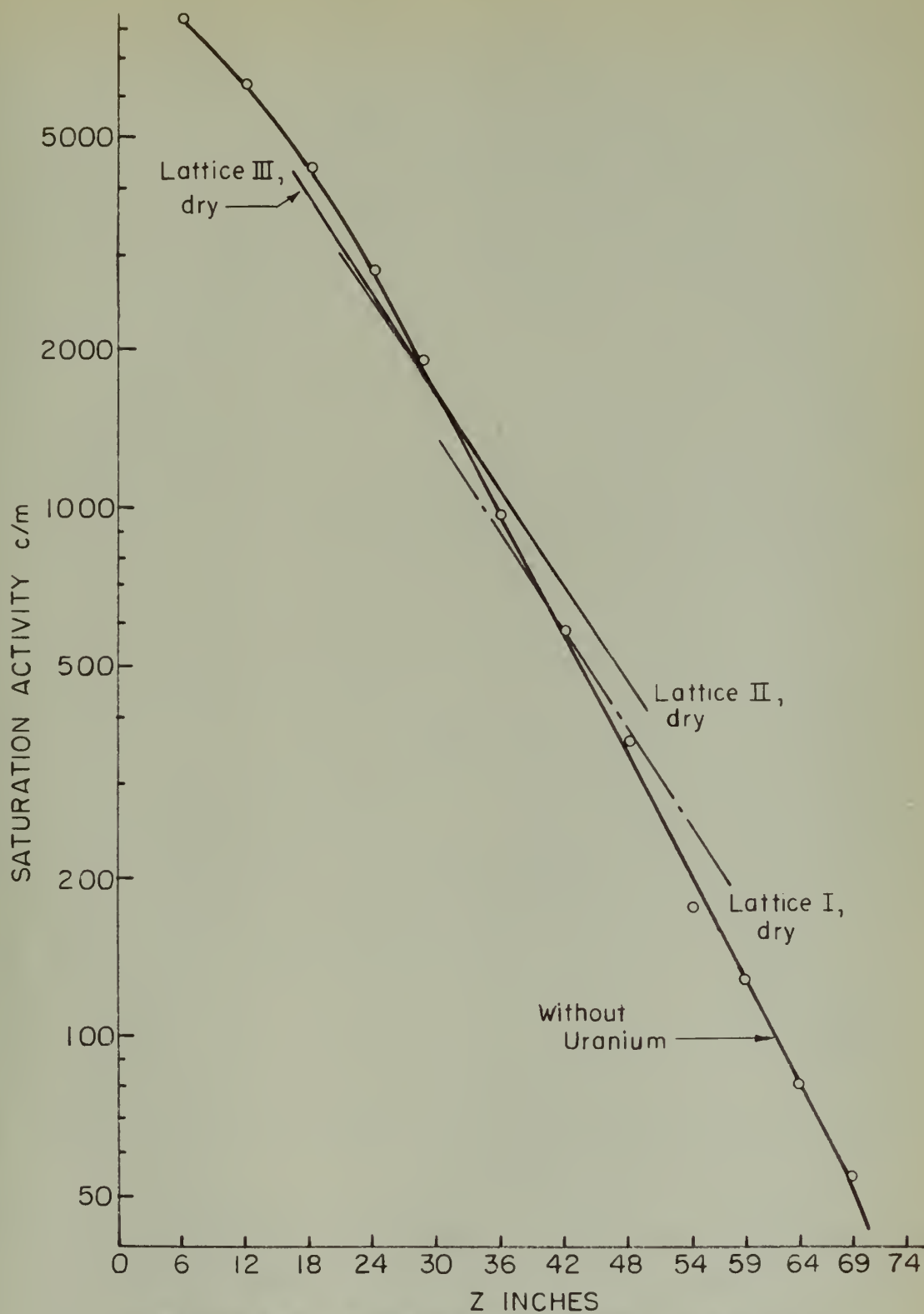


Figure 12. Vertical flux survey comparison,
 $x = 27$ in., $y = 30$ in.

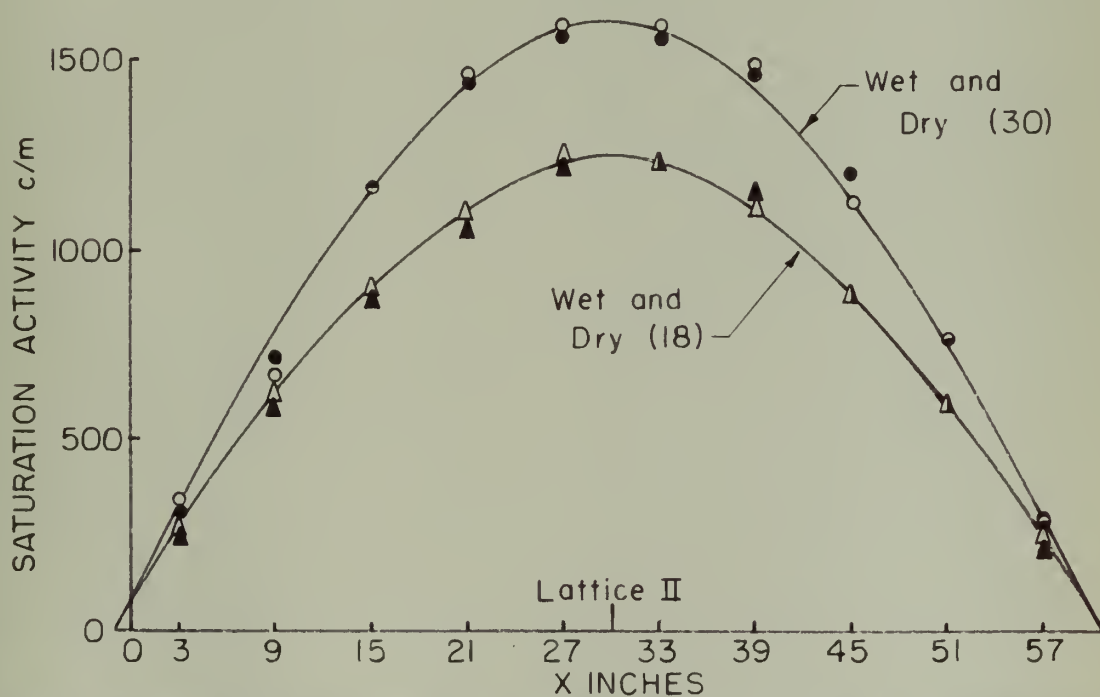
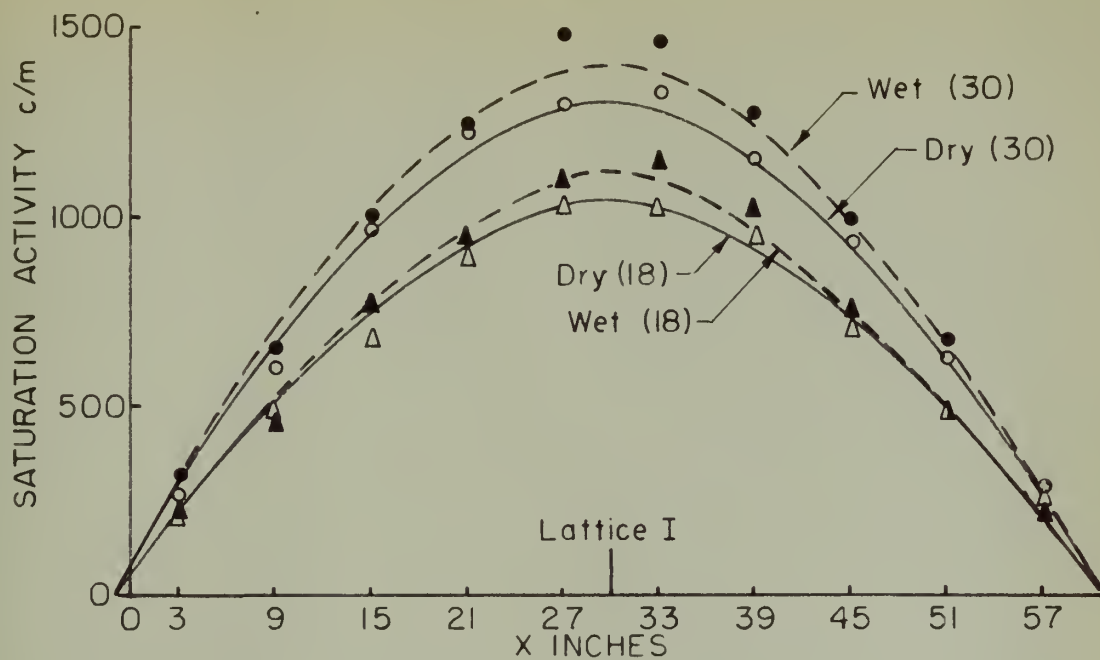


Figure 13. Horizontal flux survey, x direction, Lattice I and II, $z = 30$ in., $y = 18$ in. and $y = 30$ in.

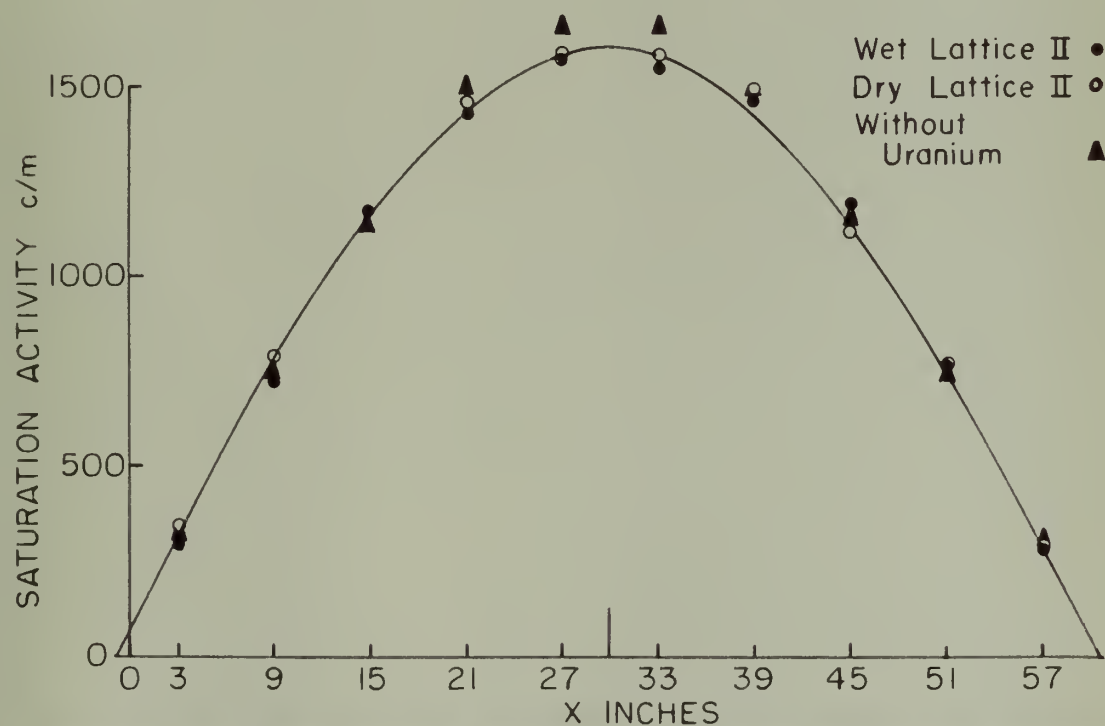
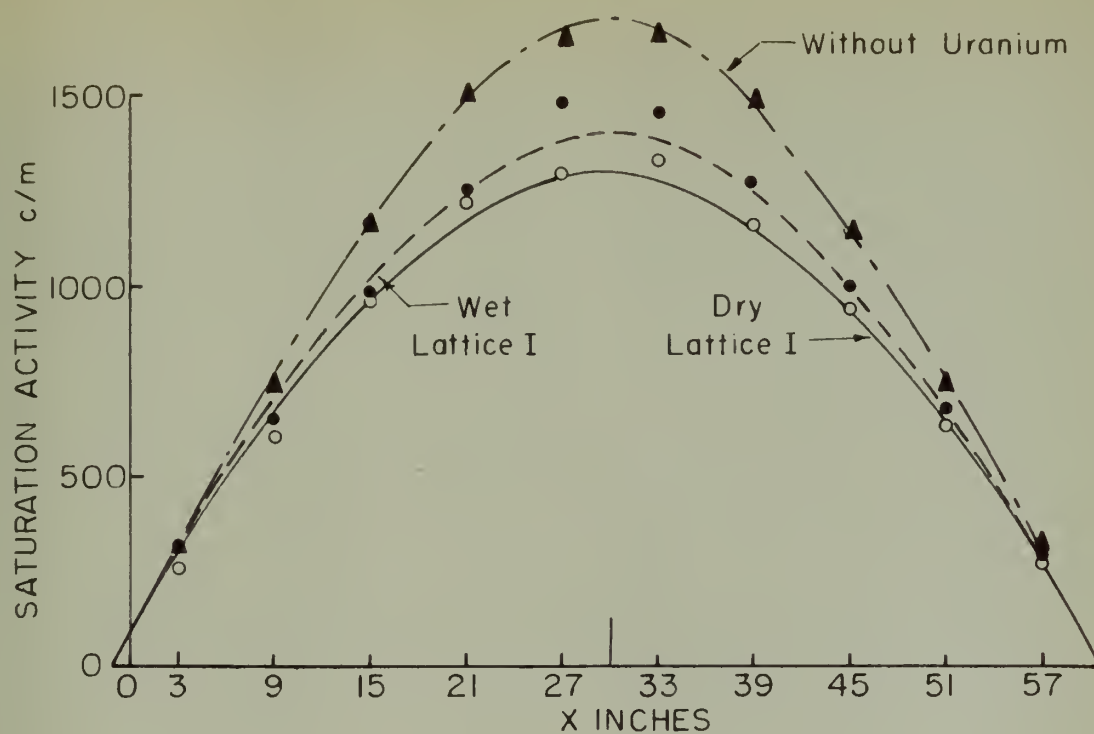


Figure 14. Horizontal survey, x direction, configuration comparison, $y = z = 30$ in.

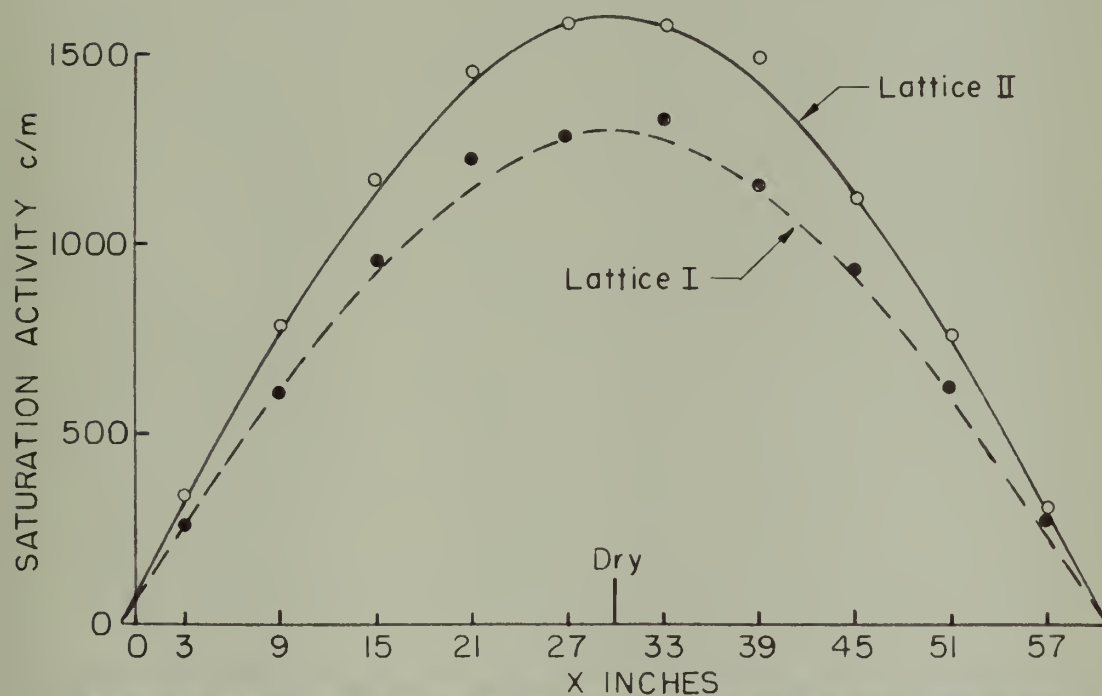
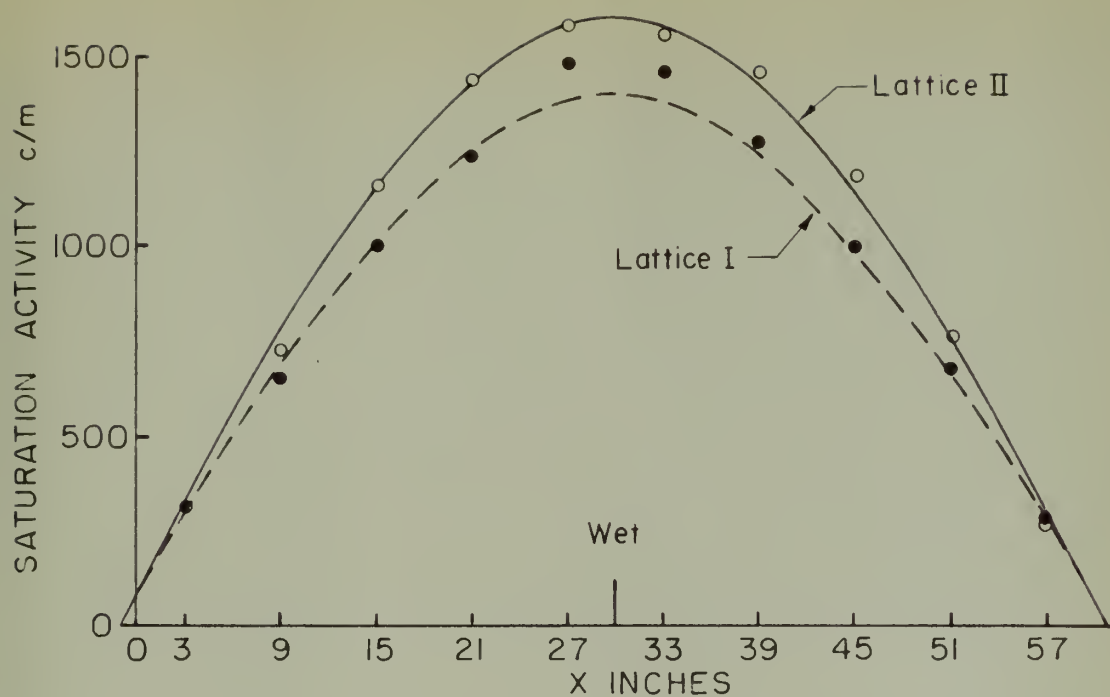


Figure 15. Horizontal survey, x direction, Lattice comparison, $y = z = 30$ in.

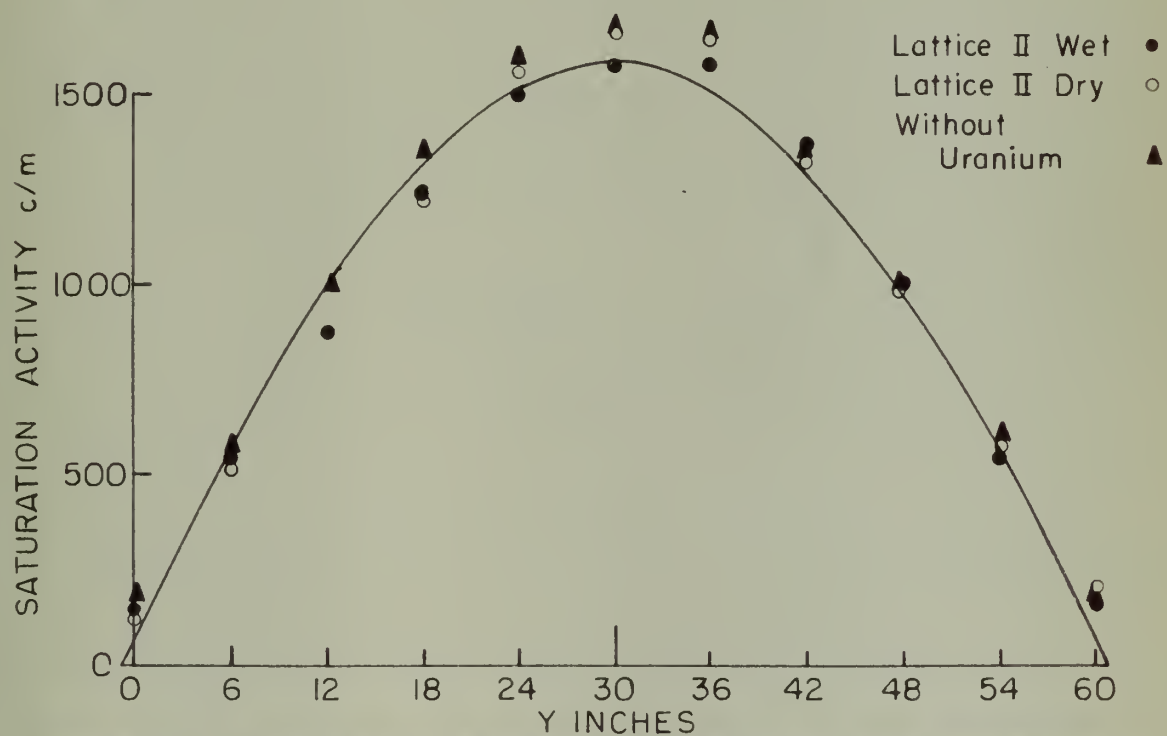
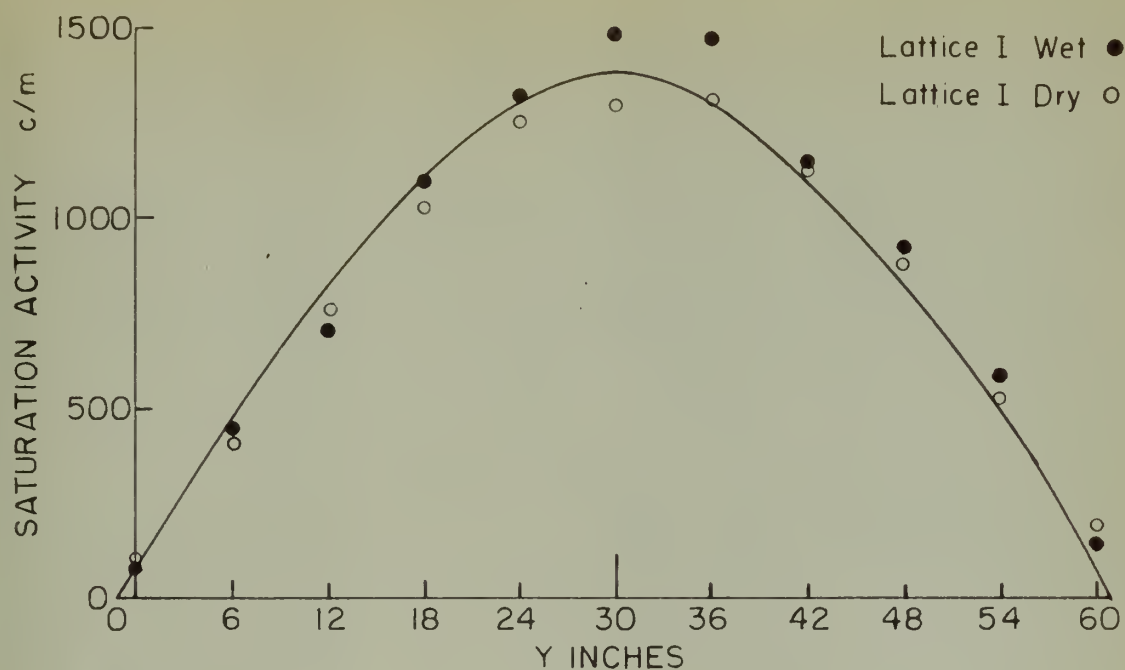


Figure 16. Horizontal survey, y direction, configuration comparison, $x = 27$ in., $z = 30$ in.

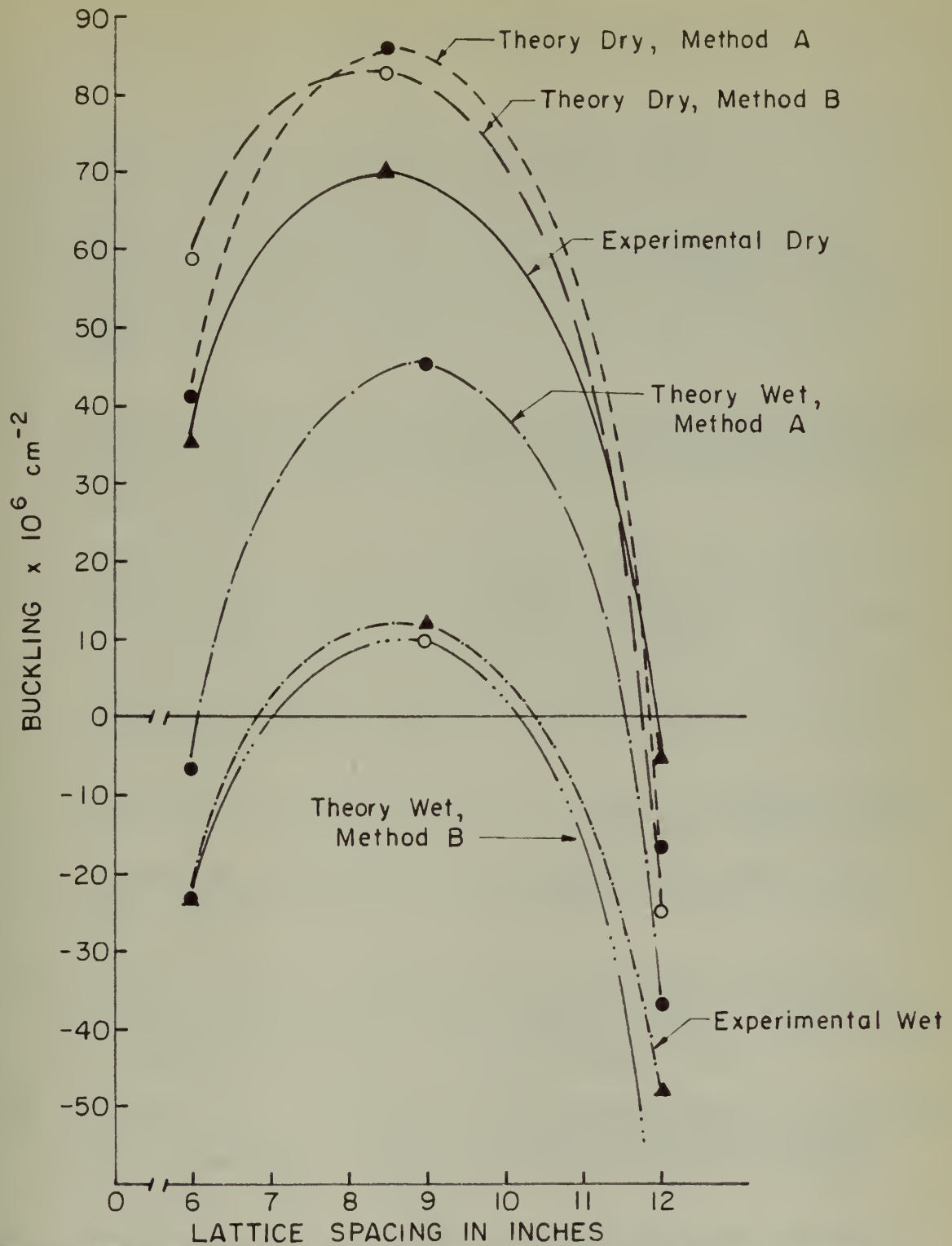


Figure 17. Theoretical and experimental buckling curves.



VIII. LITERATURE CITED

1. Murray, Raymond L. Nuclear reactor physics. Englewood Cliffs, N. J. Prentice-Hall, Inc. 1957.
2. Gast, Paul F. Normal uranium, graphite-moderated reactors: a comparison of theory and experiment—water cooled lattices. Proceedings of the International Conference on the Peaceful Uses of Atomic Energy. Vol. 5, Paper P/607, pp. 288-294, New York, United Nations. 1956.
3. Richey, C. R. Thermal unitization and lattice diffusion length in graphite-uranium lattices from exponential pile measurements. Atomic Energy Commission Document 3675. Richland, Washington, Hanford Atomic Products Operation. April 1, 1954.
4. Weinberg, A. M. Calculation of neutron distribution in heterogeneous piles. In Goodman, Clark. Ed., The science and engineering of nuclear power, Vol. 2, Chap. 6. Cambridge, Mass. Addison-Wesley Press. 1949.
5. Glasstone, Samuel and Edlund, Milton C., The elements of nuclear reactor theory. Princeton, N. J. D. Van Nostrand Co., Inc. 1952.
6. Guggenheim, E. A. and Pryce, M. H. L. Uranium-graphite lattices. Nucleonics, 11, No. 2: 50-60. February 1953.
7. Houston, R. W. Calculating thermal utilization for large thermal reactors. Nucleonics, 13, No. 4: 70-73. April 1955.
8. Davenport, D. M. Exponential experiments in graphite systems. Proceedings of the International Conference on the Peaceful Uses of Atomic Energy. Vol. 5, Paper P/599, pp. 309-316, New York, United Nations. 1956.
9. Clayton, E. D. Exponential pile measurements in graphite-uranium lattices. Atomic Energy Commission Document 3677. Richland, Washington, Hanford Atomic Products Operation. June 1, 1954.
10. Littler, D. J. and Raffle, J. F. An introduction to reactor physics. New York, McGraw Hill Book Co., Inc. 1955.

11. Glasstone, Samuel. Principles of nuclear reactor engineering. Princeton, N. J. Van Nostrand Co., Inc. 1955.
12. Table of the Bessel Functions $J_0(z)$ and $J_1(z)$ for complex arguments. Mathematical Tables Project of the National Bureau of Standards. New York, Columbia University Press, 1943.

11- *Gramma, Henry. (1901) The history of the city of New York, from its first settlement to the present time. New York: The Century Company, 1901.*

12- *Table of the population of the city of New York, from 1790 to 1900. New York: The City of New York, 1901.*

IX. ACKNOWLEDGEMENTS

I wish to express my thanks to Dr. Glenn Murphy for his original suggestion of this problem and for the loan of certain apparatus used in the experimental part of this investigation.

I wish also to express my thanks and appreciation to Dr. Robert Uhrig for his guidance and help during both the theoretical and experimental portions of this investigation.

My work at Iowa State College was my final year of study in the Aeronautical Engineering Curriculum of the United States Naval Postgraduate School, Monterey, California. I would, therefore, like to express my appreciation to the Naval Postgraduate School for making my work at Iowa State College possible.

X. APPENDIX

Table 5

Vertical flux survey Lattice I

Saturation Activity			Saturation Activity		
Position	C/M		Position	C/M	
	DRY	WET		DRY	WET
E1-18	3903	4350	E1-30	6508	7180
E2-18	3040	3395	E2-30	4580	5110
E3-18	2192	2460	E3-30	3170	3493
E4-18	1580	1681	E4-30	2085	2250
E5-18	1029	1095	E5-30	1290	1482
E6-18	716	707	E6-30	888	870
E7-18	465	478	E7-30	552	620
E8-18	335	313	E8-30	376	378
E9-18	238	230	E9-30	268	253
E10-18	135	115	E10-30	163	158
E11-18	107	91	E11-30	129	146
E12-18	59	62	E12-30	69	74
E13-18	28	32	E13-30	44	56

Table 1

Summary of the data used in the analysis

Observed data			Simulated data		
θ			θ		
θ_1	θ_2	θ_3	θ_1	θ_2	θ_3
0.1	0.2	0.3	0.1	0.2	0.3
0.2	0.3	0.4	0.2	0.3	0.4
0.3	0.4	0.5	0.3	0.4	0.5
0.4	0.5	0.6	0.4	0.5	0.6
0.5	0.6	0.7	0.5	0.6	0.7
0.6	0.7	0.8	0.6	0.7	0.8
0.7	0.8	0.9	0.7	0.8	0.9
0.8	0.9	1.0	0.8	0.9	1.0
0.9	1.0	1.1	0.9	1.0	1.1
1.0	1.1	1.2	1.0	1.1	1.2
1.1	1.2	1.3	1.1	1.2	1.3
1.2	1.3	1.4	1.2	1.3	1.4
1.3	1.4	1.5	1.3	1.4	1.5
1.4	1.5	1.6	1.4	1.5	1.6
1.5	1.6	1.7	1.5	1.6	1.7

Table 6

Horizontal flux survey Lattice I

Saturation Activity			Saturation Activity		
Position	C/M		Position	C/M	
	DRY	WET		DRY	WET
A5-18	208	226	A5-30	256	321
B5-18	489	469	B5-30	605	650
C5-18	678	765	C5-30	958	990
D5-18	893	950	D5-30	1223	1237
E5-18	1029	1095	E5-30	1290	1482
F5-18	1030	1145	F5-30	1330	1453
G5-18	952	1020	G5-30	1163	1270
H5-18	705	748	H5-30	939	994
I5-18	505	504	I5-30	629	671
J5-18	214	223	J5-30	272	282
E5-0	115	73	E5-36	1306	1465
E5-6	412	442	E5-42	1131	1131
E5-12	759	709	E5-48	875	914
E5-18	1029	1095	E5-54	525	583
E5-24	1247	1320	E5-60	180	150

Table 1
 Estimated mean values of the parameters

Parameters of the first component			Parameters of the second component		
λ_1			λ_2		
μ_1	σ_1	τ_1	μ_2	σ_2	τ_2
1.2	0.5	0.45	0.8	0.4	0.35
0.8	0.4	0.35	0.6	0.3	0.3
0.6	0.3	0.3	0.5	0.2	0.25
0.4	0.2	0.25	0.4	0.2	0.2
0.3	0.1	0.2	0.3	0.1	0.15
0.2	0.1	0.15	0.2	0.1	0.1
0.1	0.05	0.1	0.1	0.05	0.05
0.05	0.02	0.05	0.05	0.02	0.02
0.02	0.01	0.01	0.02	0.01	0.01
0.01	0.005	0.005	0.01	0.005	0.005
0.005	0.002	0.002	0.005	0.002	0.002
0.002	0.001	0.001	0.002	0.001	0.001
0.001	0.0005	0.0005	0.001	0.0005	0.0005
0.0005	0.0002	0.0002	0.0005	0.0002	0.0002
0.0002	0.0001	0.0001	0.0002	0.0001	0.0001
0.0001	0.00005	0.00005	0.0001	0.00005	0.00005
0.00005	0.00002	0.00002	0.00005	0.00002	0.00002
0.00002	0.00001	0.00001	0.00002	0.00001	0.00001
0.00001	0.000005	0.000005	0.00001	0.000005	0.000005
0.000005	0.000002	0.000002	0.000005	0.000002	0.000002
0.000002	0.000001	0.000001	0.000002	0.000001	0.000001
0.000001	0.0000005	0.0000005	0.000001	0.0000005	0.0000005
0.0000005	0.0000002	0.0000002	0.0000005	0.0000002	0.0000002
0.0000002	0.0000001	0.0000001	0.0000002	0.0000001	0.0000001
0.0000001	0.00000005	0.00000005	0.0000001	0.00000005	0.00000005
0.00000005	0.00000002	0.00000002	0.00000005	0.00000002	0.00000002
0.00000002	0.00000001	0.00000001	0.00000002	0.00000001	0.00000001
0.00000001	0.000000005	0.000000005	0.00000001	0.000000005	0.000000005

Table 7

Vertical flux survey Lattice II

Position	Saturation Activity C/M		Position	Saturation Activity C/M	
	DRY	WET		DRY	WET
E1-18	4590	4900	E1-30	7400	7815
E2-18	3665	3802	E2-30	5505	5690
E3-18	2720	2790	E3-30	3768	3975
E4-18	1899	1930	E4-30	2680	2607
E5-18	1241	1235	E5-30	1583	1571
E6-18	801	784	E6-30	1009	1049
E7-18	536	499	E7-30	707	651
E8-18	376	332	E8-30	440	453
E9-18	255	208	E9-30	282	278
E10-18	135	147	E10-30	175	180
E11-18	111	98	E11-30	135	118
E12-18	79	61	E12-30	100	96
E13-18	35	38	E13-30	50	46

Table 8
Horizontal flux survey Lattice II

Saturation Activity			Saturation Activity		
Position	C/M		Position	C/M	
	DRY	WET		DRY	WET
A5-18	262	252	A5-30	340	304
B5-18	632	607	B5-30	791	728
C5-18	898	926	C5-30	1170	1169
D5-18	1105	1055	D5-30	1456	1435
E5-18	1241	1235	E5-30	1583	1571
F5-18	1230	1227	F5-30	1578	1550
G5-18	1111	1156	G5-30	1487	1460
H5-18	891	886	H5-30	1120	1189
I5-18	602	595	I5-30	762	759
J5-18	266	221	J5-30	308	291
E5-0	117	148	E5-36	1641	1572
E5-6	511	541	E5-42	1347	1360
E5-12	887	874	E5-48	965	1002
E5-18	1241	1235	E5-54	576	535
E5-24	1550	1499	E5-60	195	160

Table 9
Vertical flux survey Lattice III

Position	Saturation Activity	
	C/M	
	DRY	WET
E1-30	7500	7985
E2-30	5945	6150
E3-30	3960	3990
E4-30	2813	2742
E5-30	1660	1658
E6-30	1152	1093
E7-30	669	637
E8-30	458	425
E9-30	265	234
E10-30	184	153
E11-30	148	118
E12-30	79	51
E13-30	49	56

Table 10

Lattice flux survey without uranium

Position	Saturation Activity C/M	Position	Saturation Activity C/M
E1-30	8365	E5-0	172
E2-30	6290	E5-6	568
E3-30	4408	E5-12	992
E4-30	2795	E5-18	1339
E5-30	1655	E5-24	1590
E6-30	965	E5-36	1639
E7-30	587	E5-42	1320
E8-30	361	E5-48	990
E9-30	176	E5-54	615
E10-30	128	E5-60	183
E11-30	81		
E12-30	54		
E13-30	22		
A5-30	320	G5-30	1486
B5-30	736	H5-30	1143
C5-30	1161	I5-30	735
D5-30	1500	J5-30	318
F5-30	1669		



JA 17 58
7 Sept. 59

BINDERY
INTERLIB
AEC

Thesis
H677

Hoganson

35884

Operating characterist-
ics of a uranium graphite
subcritical assembly with
coolant simulation.

JA 17 58
7 Sept. 59

BINDERY
INTERLIB
AEC

t-
te
th

Thesis
H677

Hoganson

35884

Operating characteristics of a
uranium graphite subcritical
assembly with coolant simulation

thesH677

Operating characteristics of a uranium g



3 2768 002 06867 8

DUDLEY KNOX LIBRARY